

AUV STATE ESTIMATION, NAVIGATION, AND CONTROL IN THE  
PRESENCE OF OCEAN CURRENTS

A Thesis

Presented in Partial Fulfilment of the Requirements for the

Degree of Master of Science

with a

Major in Mechanical Engineering

in the

College of Graduate Studies

University of Idaho

by

Joseph Osborn

Major Professor: Eric Wolbrecht, Ph.D.

Committee Members: Michael Anderson, Ph.D.; Dean Edwards, Ph.D.

Department Administrator: Steven Beyerlein, Ph.D.

May 2016

## Authorization To Submit Thesis

This thesis of Joseph Osborn, submitted for the degree of Master of Science with a Major in Mechanical Engineering and titled “AUV State Estimation, Navigation, and Control in the Presence of Ocean Currents,” has been reviewed in final form. Permission, as indicated by the signatures and dates below, is now granted to submit final copies to the College of Graduate Studies for approval.

Major Professor \_\_\_\_\_ Date \_\_\_\_\_  
Eric Wolbrecht, Ph.D.

Committee  
Members \_\_\_\_\_ Date \_\_\_\_\_  
Michael Anderson, Ph.D.

\_\_\_\_\_  
Date \_\_\_\_\_  
Dean Edwards, Ph.D.

Department  
Administrator \_\_\_\_\_ Date \_\_\_\_\_  
Steven Beyerlein, Ph.D.

## **Abstract**

The ability to make oceanographic scientific measurements without the need for fixed hardware is of interest to the US Navy. The Office of Naval Research (ONR) has been exploring the feasibility of using autonomous underwater vehicles (AUVs) to conduct such measurements. To this end, the University of Idaho (UI) has developed a fleet of AUVs.

To better operate in the presence of ocean currents, the UI AUVs have been equipped with a higher powered motor. As AUV operations increased in speed, the control gains have been investigated through the use of simulation and field testing to achieve more stable performance.

When making scientific measurements it is crucial to both temporally and spatially localize the AUVs. To accomplish this an extended Kalman filter (EKF) is employed to estimate the position and orientation of the UI AUVs. To improve this state estimation in oceanic environments, a new EKF was designed to directly estimate the ocean currents. These estimated currents have been utilized to adapt the heading controller to account for the effects of these currents. Additionally, to improve operations in an oceanic environment the AUVs have been programmed to propagate a continuous EKF for a set of chained missions, allowing multiple missions to be conducted without the need for operator input.

The new EKF and adapted heading controller were simulated and subsequently field tested. Although simulation results were promising, an ineffective speed correlation caused large estimation divergence during field testing. Despite this divergence, the EKF accurately estimated currents in field testing suggesting that the concept of estimating currents and leveraging these estimates to improve navigation is feasible.

## **Acknowledgements**

I would like to thank my major professor, Dr. Wolbrecht, who has been a huge help throughout my research. Additionally, I would like to thank Dr. Anderson, who has been an amazing help in so many ways, and without whom I would not have been in graduate school. Without the work of everyone involved on this project, both past and present, I would not have been able to accomplish what I have.

I would especially like to thank my family who have supported me through everything in life. Without them I would not have the tremendous opportunities in life that I have been fortunate enough to have.

## Table of Contents

<b>Authorization to Submit Thesis</b> . . . . .	<b>ii</b>
<b>Abstract</b> . . . . .	<b>iii</b>
<b>Acknowledgements</b> . . . . .	<b>iv</b>
<b>Table of Contents</b> . . . . .	<b>v</b>
<b>List of Acronyms</b> . . . . .	<b>viii</b>
<b>List of Tables</b> . . . . .	<b>ix</b>
<b>List of Figures</b> . . . . .	<b>x</b>
<b>1 Introduction</b> . . . . .	<b>1</b>
1.1 Project Overview . . . . .	1
1.2 Ocean Currents . . . . .	2
<b>2 Methods</b> . . . . .	<b>3</b>
2.1 University of Idaho AUVs . . . . .	3
2.2 AUV Control Gains . . . . .	4
2.2.1 Simulation . . . . .	5
2.2.2 Field Testing . . . . .	5
2.3 Chained-Missions Continuous EKF . . . . .	6
2.4 Extended Kalman Filter . . . . .	7
2.5 Current Estimation EKF . . . . .	9
2.6 EKF Covariance Matrices . . . . .	14
2.6.1 Process Noise Covariance Matrix . . . . .	15
2.6.2 Measurement Noise Covariance Matrix . . . . .	16

2.6.3	State Covariance Matrix . . . . .	17
2.7	MOOS Heading Controller . . . . .	19
2.8	Modified MOOS Heading Controller . . . . .	20
2.9	Estimation and Navigation Simulations . . . . .	22
2.10	Estimation and Navigation Field Testing . . . . .	23
2.10.1	Zero Current . . . . .	24
2.10.2	Simulated Current . . . . .	24
<b>3</b>	<b>Results &amp; Discussion . . . . .</b>	<b>26</b>
3.1	AUV Control Gains Testing . . . . .	26
3.1.1	Simulation . . . . .	26
3.1.2	Field Testing . . . . .	29
3.2	Chained-Missions Continuous EKF Field Test . . . . .	32
3.3	Estimation and Navigation Simulation Results . . . . .	35
3.3.1	Zero Current . . . . .	36
3.3.2	Constant Current . . . . .	40
3.4	Estimation and Navigation Field Testing Results . . . . .	45
3.4.1	Zero Current . . . . .	45
3.4.2	Simulated Current . . . . .	48
<b>4</b>	<b>Conclusions . . . . .</b>	<b>51</b>
4.1	Future Work . . . . .	53
4.1.1	CFD Model . . . . .	53
4.1.2	Speed Correlation . . . . .	53
4.1.3	Covariance Matrices . . . . .	54
	<b>References . . . . .</b>	<b>57</b>
	<b>Appendix A: Dynamic Model Force and Moment Equations . . . . .</b>	<b>58</b>

**Appendix B: Modified MOOS Heading Controller Calculation . . . . . 65**

## List of Acronyms

<b>ARD</b>	Acoustic Research Detachment
<b>AUV</b>	Autonomous Underwater Vehicle
<b>EKF</b>	Extended Kalman Filter
<b>IMU</b>	Inertial Measurement Unit
<b>LBL</b>	Long Baseline
<b>MOOS</b>	Mission Oriented Operating Suite
<b>MSBL</b>	Moving Short Base
<b>ONR</b>	Office of Naval Research
<b>SOG</b>	Speed Over Ground
<b>STW</b>	Speed Through Water
<b>UI</b>	University of Idaho
<b>VOG</b>	Velocity Over Ground
<b>VTW</b>	Velocity Through Water



**List of Tables**

3.1	RMS depth error from field testing . . . . .	30
3.2	RMS heading error from field testing . . . . .	32
3.3	Field test estimation and navigation errors in zero current . . . . .	47
3.4	Field test estimation and navigation errors with a simulated current . . . . .	50

## List of Figures

2.1	Picture of a UI AUV . . . . .	3
2.2	Vector addition of VTW and ocean currents to calculate VOG . . . . .	12
2.3	Original MOOS heading control . . . . .	20
2.4	The Modified MOOS Heading Controller . . . . .	21
3.1	Proportional pitch and depth gains parametric study simulation output . . . . .	27
3.2	Proportional heading gain simulation output . . . . .	28
3.3	Proportional pitch and depth gains parametric study field testing . . . . .	30
3.4	Proportional heading gain field testing . . . . .	31
3.5	Chained mission continuous EKF estimate field test . . . . .	33
3.6	Previous EKF simulation in zero current . . . . .	37
3.7	New EKF simulation in zero current . . . . .	38
3.8	New EKF with modified MOOS controller simulation in zero current . . . . .	39
3.9	Previous EKF simulation in a constant current . . . . .	41
3.10	New EKF simulation in a constant current . . . . .	42
3.11	New EKF with modified MOOS controller simulation in zero current . . . . .	43
3.12	Field test of the new EKF in zero current . . . . .	46
3.13	Field test of the new EKF using a simulated current . . . . .	49

## Chapter 1: Introduction

Portions of this chapter appear in the following:

J. Osborn, S. Qualls, J. Canning, M. Anderson, D. Edwards and E. Wolbrecht, "AUV State Estimation and Navigation to Compensate for Ocean Currents," *OCEANS 2015 - MTS/IEEE Washington*, Washington, DC, 2015, pp. 1-5.

### 1.1 Project Overview

The ability to make scientific measurements in ocean environments is of particular interest to the US Navy. One approach the Office of Naval Research (ONR) is exploring is equipping autonomous underwater vehicles (AUVs) with a variety of sensors in order to conduct oceanographic survey measurements. In response to this need, the University of Idaho (UI) has created a fleet of AUVs with the goal of performing such measurements.

Oceanic survey measurements require both accurate sensing technology and localization. That is, a measurement only has value if its time, location, and orientation are accurately known. When using AUVs to conduct such measurements this requires accurate knowledge of position and orientation to be temporally synced with each acquired measurement. Presently each UI AUV uses an extended Kalman filter (EKF) to estimate its own position (north and east), speed, and heading as it navigates. This EKF utilizes range measurements from a long-baseline (LBL) array of transponders at known locations as well as heading and propeller speed measurements from onboard sensors. For navigation, the EKF position estimate is leveraged to keep the AUV on course through the use of a Mission Oriented Operating Suite (MOOS) heading controller [1].

Previous research has led to the development of several distinct EKF schemes for state estimation on the UI AUVs. The basic LBL EKF [2] was previously augmented with an additional state to improve navigation in the presence of strong magnetic fields that can induce a false compass reading [3]. Further research was focused on increasing portability by

eliminating the need for a bottom mounted LBL array. Additional research explored the use of ship mounted transponder arrays in various geometries termed moving short baseline (MSBL) navigation [4], as well as attempts to increase the accuracy of these MSBL navigation schemes with the use of an additional support transponder, referred to as hybrid baseline navigation (HBL) [5].

## 1.2 Ocean Currents

A notable challenge with AUV state estimation in oceanic environments is the lack of ground truth for speed measurement. A Doppler velocity log (DVL) may be used to acquire high-accuracy absolute-velocity measurements [6], but their large physical size and high cost make them unsuitable for the UI AUVs. Presently, speed measurement for an UI AUV is determined from a correlation to propeller speed (RPM). Unlike the DVL, this is a relative-speed measurement, referred to herein as speed through water (STW). STW is a good estimate of speed over ground (SOG) when water currents are negligible, but this is not the case in most ocean environments.

Previous approaches to navigation in ocean currents includes control based methods such as Lyapunov based adaptive control [7] and multivariable sliding mode control [8]. Another common approach, typically for ocean gliders, focuses on path planning [9, 10]. In [11] water current disturbances are estimated from the AUVs perturbed position. For the present application, state estimation is paramount, and thus we have developed an approach that first directly estimates water current as states in an EKF, similar to [12, 13]. Next, the water-current estimates are used separately for navigation and control.

## Chapter 2: Methods

### 2.1 University of Idaho AUVs

The UI AUVs are based on the Virginia Polytechnic Institute AUV [14], which was designed to be low cost and easily deployed. These AUVs are small and lightweight; about 1m in length, 10cm in diameter. This allows them to be deployed by a single person, increasing the flexibility of their use. More details on the UI AUV design can be found in [15].

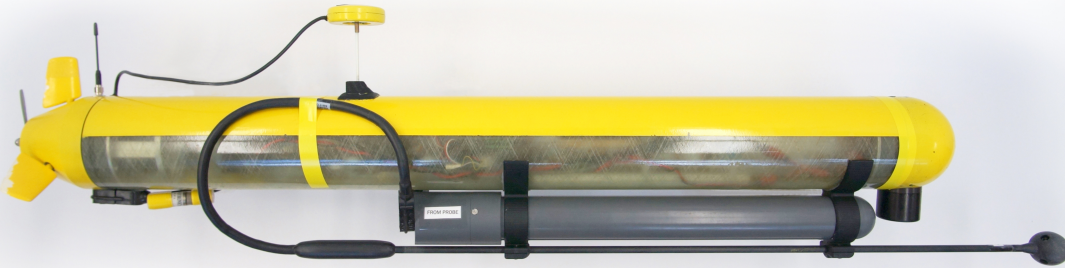


**Figure 2.1:** Picture of a UI AUV equipped with electric field probe and preamplifier.

Several sensors and various hardware are incorporated into the AUV for necessary processes including communication and navigation. Included in these are: a Woods Hole Oceanographic Institution (WHOI) micro-modem used for acoustic communication and LBL navigation pings; a capacitive pressure transducer used to measure depth; a GPS unit for surface positioning; an inertial measurement unit (IMU) for angular rates of change; a magnetic compass for heading measurement; and a radio antenna for real-time telemetry data and remote operation. For more detail of on-board sensors see [2].

Previous research conducted with the UI AUVs include fleet operations [16] and magnetic signature measurements [17, 18]. Presently these AUVs are being used to investigate the feasibility of making oceanographic electric field measurements. In Figure 2.1 an electric field probe and accompanying preamplifier can be seen attached to the bottom of the AUV. As research progresses, it is desired to expand all these operations to an oceanic environment.

This will increase their flexibility of use. Additionally, it will provide a conductive medium for electric field measurements.

## 2.2 AUV Control Gains

To improve the ability to operate in oceanic environments, the AUVs were upgraded to a more powerful motor of roughly the same physical size. This allows for higher speed operations, which is beneficial for making headway against currents. To maintain stable control, the control gains had to be adapted for operations at these higher speeds. The previous AUV motor typically operated at 1000RPM, and thus the control gains were optimized for operation at this rate.

Due to the nature of the AUV dynamics, all three control values considered (heading, pitch and depth) are coupled. To reduce the complexity, the heading was considered independent from the pitch and depth control. To treat these cases independently, the roll angle of the sub is assumed negligible. Although this may not be the case in actual operation, it allows for simplicity when investigating the general trends associated with a perturbation to one of the control values. As pitch and depth are both controlled by the same input, they cannot be treated as uncoupled.

Both pitch and depth are controlled by the elevators. This convolutes the control issue as it creates a single input, multiple output system. As the AUVs have a slight positive buoyancy, it is desired to be at the set depth with a slight downward pitch. As the set pitch is not perfectly calibrated for the operational speeds, a dynamic control system that has no steady-state solution is produced. This induces a complex interplay between the proportional gains on pitch and depth. Ideally, oscillations about the set depth will be minimized.

The heading is controlled by the rudder. When treating the system as uncoupled this is a single input, single output system, which makes the analysis less complicated. Some complication arises when extended to implementation on the AUV as there is asymmetric hydrodynamic drag with the externally mounted electric field measurement system hardware.

Based on the configuration of the measurement system, this asymmetry can be slight to severe. As it is desired to have a single set of gains that work for all configurations of the AUV, the heading gain will be investigated across several of these configurations.

### 2.2.1 Simulation

A dynamic simulation based on the equations presented in Appendix A was used for the first analysis of the control gains. This simulation uses an uncoupled, simplified, geometry-based, hydrodynamic model of the AUV. With this simplified model the predicted behavior will not match the AUV behavior exactly, yet the general trends should be similar. Thus, the simulation will give an idea of which way to perturb the gains for beneficial results. As the simulation is uncoupled, the heading is treated separately from the pitch and depth.

For the pitch and depth gains, a parametric study was conducted that used the previous standard gains along with perturbed values both larger and smaller. As the pitch and depth are highly coupled, analyzing the depth alone is sufficient for ensuring stability of both states. Thus, only the depth was analyzed for magnitude and frequency of oscillation.

With the heading gain, there was only one parameter to change. As with the depth and pitch gains, the previous standard gain was compared to gains perturbed both larger and smaller. The heading was analyzed similar to the depth to decide which way to tune the gain for beneficial behavior.

### 2.2.2 Field Testing

With the trends predicted by the simulation, various gain combinations were selected as viable options for implementation on the AUVs for field testing. As a basis for comparison, the original gains were included. Parametric studies were conducted during field testing to independently evaluate the performance of the various gains for both depth and heading. Missions were performed at the extremes of operational motor RPM, 800 and 1500 RPM, as well as the previous standard of 1000 RPM for all the permutations of gains. The recorded

sensor measurements from these various tests were compared and evaluated based on magnitude and frequency of oscillations during semi-steady-state operation. These test were used to establish new gains for use across all operational speeds.

### **2.3 Chained-Missions Continuous EKF**

For further improvement of operations in oceanic environments the AUVs were programmed to be able to conduct several missions sequentially from one mission start command, referred to as chained missions. This improves field testing operations as previously only one mission could be commanded, then the AUV would remain passive until radio contact was established and a new mission started or the control was taken over remotely by joystick. During this time, the AUV is carried by the current.

With the AUVs now being able to execute chained missions, it was necessary to keep a continuous EKF estimate. This is important as there is no guarantee that the AUV will be on the surface at the start of a LBL mission, which uses the EKF estimate for navigation. Without being on the surface, the EKF cannot be accurately initialized. The logical solution is to initialize the EKF on the surface with the first mission in a set of chained missions and keep a continuous EKF estimate of the AUV location.

With the implementation of the chained missions, a flag in the on-board code was included to communicate the presence of chained missions on the AUV. Leveraging this, the EKF is initialized based on this flag for any mission type. For simplicity, the EKF will be propagated regardless of whether or not there is an LBL mission in the set of chained missions. This simplifies the implementation as well as gives more testing of the EKF. To correctly implement the chained-mission continuous EKF, the AUV source code had to be modified to update the EKF across all mission types. The different mission types that are implemented on the AUVs are: GPS missions which utilize the GPS position for navigation; LBL missions which navigate based on the EKF estimated position; and timed missions which are either open-loop control, which control to a set rudder angle, or closed-loop control, which control to a set heading based



on the measured compass heading. As the EKF wasn't previously used on the mission modes that don't use the estimate for navigation, there were no measurement updates sent to the EKF. These measurement updates are vital to the accuracy of the EKF.

To validate that the chained-missions continuous EKF was working properly, field tests were conducted. As the EKF will need to propagate correctly across all mission types, a test was conducted that utilized all the different types of missions used.

## 2.4 Extended Kalman Filter

Rudolph Kalman provided the mathematical basis of an optimal linear filter, which would come to be known as the Kalman Filter, in 1960 in [19, 20]. This filter works on the assumption that a system model and associated measurement model can be accurately represented as linear, and that any noise that perturbs the system is additive white noise. As most real dynamic systems are nonlinear, nor can be accurately approximated as such, much work has been put into developing nonlinear filters. One of the most widely used of these nonlinear filtering methods is the extended Kalman filter (EKF), which uses a first order multivariate Taylor's expansion about the estimation point. This results in linear approximations of the propagation and measurement models in the neighborhood of the current state estimate. With these linear model approximations, the linear Kalman filter equations can be used. Additionally, the assumption that the noise is additive is relaxed in the EKF.

Using the notation from [21], the steps of the EKF are as follows. The extended Kalman filter is applied to a nonlinear system denoted as

$$x_k = f_{k-1}(x_{k-1}, u_{k-1}, w_{k-1}), \quad (2.1)$$

with associated measurement model

$$y_k = h_k(x_k, v_k), \quad (2.2)$$

where subscript  $k$  denotes the time step;  $x$  is the state vector;  $f$  is the nonlinear propagation model;  $h$  is the nonlinear measurement model;  $u$  is the system inputs;  $w$  and  $v$  are white noise with known covariance matrices  $Q$  and  $R$ , such that

$$w_k \sim (0, Q_k); \quad (2.3)$$

$$v_k \sim (0, R_k). \quad (2.4)$$

The filter is initialized with

$$\hat{x}_0^+ = E(x_0); \quad (2.5)$$

$$P_0^+ = E \left[ (x_0 - \hat{x}_0^+) (x_0 - \hat{x}_0^+)^T \right], \quad (2.6)$$

where  $E$  denotes the expected values.  $\hat{x}^+$  is the *a posteriori* estimate of the state and  $P^+$  is the covariance associated with this estimate. The filter is then propagated to the next time step by first linearizing the propagation model about the estimated state and noise, i.e.

$$F_{k-1} = \left. \frac{\partial f_{k-1}}{\partial x} \right|_{\hat{x}_{k-1}^+}; \quad (2.7)$$

$$L_{k-1} = \left. \frac{\partial f_{k-1}}{\partial w} \right|_{\hat{x}_{k-1}^+}, \quad (2.8)$$

and performing the time update to obtain the *a priori* estimates

$$\hat{x}_k^- = f_{k-1}(\hat{x}_{k-1}^+, u_{k-1}, 0); \quad (2.9)$$

$$P_k^- = F_{k-1} P_{k-1}^+ F_{k-1}^T + L_{k-1} Q_{k-1} L_{k-1}^T. \quad (2.10)$$

Next, the measurement model is linearized about this *a priori* state estimate such that

$$H_k = \left. \frac{\partial h_k}{\partial x} \right|_{\hat{x}_k^-}; \quad (2.11)$$

$$M_k = \left. \frac{\partial h_k}{\partial v} \right|_{\hat{x}_k^-}, \quad (2.12)$$

and the estimate is updated with information from the measurements to a new *a posteriori* estimate via

$$K_k = P_k^- H_k^T (H_k P_k^- H_k^T + M_k R_k M_k^T)^{-1}; \quad (2.13)$$

$$\hat{x}_k^+ = \hat{x}_k^- + K_k [y_k - h_k(\hat{x}_k^-, 0)]; \quad (2.14)$$

$$P_k^+ = (I - K_k H_k) P_k^-. \quad (2.15)$$

This is performed recursively and provides a real-time estimate of the state.

## 2.5 Current Estimation EKF

The various EKFs that have been explored for use on the UI AUVs have shown promising results in both simulation and field testing. Though these have worked well for past research, all of these EKF schemes are ineffective in oceanic environments due to the assumption that the speed through water (STW) is a sufficient estimate of the speed over ground (SOG). As all previous field testing has been conducted in Lake Pend Oreille, this assumption was safe due to negligible water movement. As operations are extended to oceanic environments, this assumption no longer holds.

As the UI AUVs have not been operated in oceanic environments prior to recent research, it is advantageous to start as simply as possible. Instead of attempting to adapt the more sophisticated EKF schemes, i.e. MSBL or HBL, for oceanic operations, the simpler and more robust bottom-mounted LBL array scheme is used. The new EKF implementation was designed from the EKF used for magnetic measurements. This was the most recently used

LBL EKF scheme. This EKF included the basic states: local east position,  $E$ ; local north position,  $N$ ; relative speed,  $s$ ; and AUV heading,  $\psi$ . In addition to these basic states, this EKF included a heading bias state,  $b$ , and a gyro measurement,  $\dot{\psi}$ , as a driving function. These were important with magnetic field measurements as the magnetic source being measured induced a bias in the compass reading. This previous EKF scheme's propagation model was

$$\begin{aligned}
 x_k = f_{k-1}(x_{k-1}, u_{k-1}, w_{k-1}) &= \begin{bmatrix} E + s \sin \psi \Delta t + w_E \\ N + s \cos \psi \Delta t + w_N \\ s + w_s \\ \psi + \dot{\psi} \Delta t + w_\psi \\ b + w_b \end{bmatrix}_{k-1} ; \\
 x &= \begin{bmatrix} E & N & s & \psi & b \end{bmatrix}^T ; \\
 u &= \dot{\psi}; \\
 w &= \begin{bmatrix} w_E & w_N & w_s & w_\psi & w_b \end{bmatrix}^T, \quad (2.16)
 \end{aligned}$$

where  $x$  is the state vector,  $f$  is the system equation,  $u$  is the driving function,  $w$  is the vector of the noise associated with each state (i.e.  $w_E$  is the noise associated with the propagation of the local east position), and  $\Delta t$  is the time step of the system model propagation. This EKF is updated with four range measurements,  $r_A$ - $r_D$ , a speed measurement,  $s_m$  and a heading measurement,  $\psi_m$ . These measurements are incorporated into the EKF via the measurement

model

$$\begin{aligned}
 y_k = h(x_k, v_k) &= \left[ \begin{array}{c} \sqrt{(E - A_E)^2 + (N - A_N)^2 + (Z - A_Z)^2} + v_A \\ \sqrt{(E - B_E)^2 + (N - B_N)^2 + (Z - B_Z)^2} + v_B \\ \sqrt{(E - C_E)^2 + (N - C_N)^2 + (Z - C_Z)^2} + v_C \\ \sqrt{(E - D_E)^2 + (N - D_N)^2 + (Z - D_Z)^2} + v_D \\ s + v_{s_m} \\ \Psi + b + v_{\Psi_m} \end{array} \right]_k ; \\
 y &= \left[ r_A \quad r_B \quad r_C \quad r_D \quad s_m \quad \Psi_m \right]^T ; \\
 v &= \left[ v_A \quad v_B \quad v_C \quad v_D \quad v_{s_m} \quad v_{\Psi_m} \right]^T ,
 \end{aligned} \tag{2.17}$$

where  $y$  is the measurement vector,  $h$  is the measurement equation,  $Z$  is the measured AUV depth,  $A_E$ ,  $A_N$ , and  $A_Z$  are the local east position, local north position and depth, respectively, of transponder A (likewise for  $B$ - $D$ ), and  $v$  is the vector of noise associated with each measurement (analogous to  $w$  in the propagation model).

With the EKF represented by Equations (2.16) and (2.17), the effects of current can be captured as a speed and heading bias. This allows the AUV to effectively estimate its position and navigate to the desired waypoint path when traveling in one direction. Unfortunately, these biases are in the AUV's local frame and any change in direction will cause degraded state estimation as new biases are learned. Further discussion on this will be undertaken in the results section.

In the EKF used on the UI AUVs, the speed measurement is based solely on the propeller RPM. Although not necessarily a good estimate of SOG, this is a valid estimate of the STW and can be utilized with an estimate of the encountered current to estimate the SOG. This is achieved with the use of the estimated heading, to get a velocity through water (VTW) estimate. This VTW estimate is combined with estimates of the currents in the east and north directions. The resultant vector is an estimated velocity over ground (VOG). Figure 2.2 shows this idea

graphically.

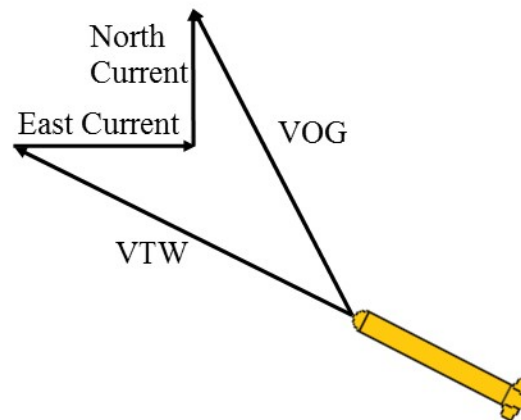


**Figure 2.2:** Vector addition of VTW and ocean currents to calculate VOG.

The new EKF implementation includes this relationship between VTW and VOG by using the east and north components of this VOG estimate for the propagation of the east and north states, respectively. This requires the addition of two states to the EKF estimate; east and north currents,  $c_E$  and  $c_N$ . The inclusion of these two additional states creates an unobservable system. To remedy this, the heading bias term was removed to reestablish observability. Without this heading bias term estimation may be degraded near large magnetic disturbances, yet, as the gyro measurement is still utilized by the EKF, this effect may be mitigated.

This new EKF is propagated through

$$\begin{aligned}
 x_k = f_{k-1}(x_{k-1}, u_{k-1}, w_{k-1}) &= \begin{bmatrix} E + s \sin \psi \Delta t + c_E \Delta t + w_E \\ N + s \cos \psi \Delta t + c_N \Delta t + w_N \\ s + w_s \\ \psi + \dot{\psi} \Delta t + w_\psi \\ c_E + w_{c_E} \\ c_N + w_{c_N} \end{bmatrix}_{k-1} ; \\
 x &= \begin{bmatrix} E & N & s & \psi & c_E & c_N \end{bmatrix}^T ; \\
 u &= \dot{\psi}; \\
 w &= \begin{bmatrix} w_E & w_N & w_s & w_\psi & w_{c_E} & w_{c_N} \end{bmatrix}^T . \quad (2.18)
 \end{aligned}$$

As can be seen in Equation (2.18), the east and north states are propagated as in Equation (2.16), but augmented with the current states ( $c_E$  and  $c_N$ ). As these water-current states are not able to be measured nor affect any of the measurements, the measurement model is not affected by the inclusion of these states. Though the inclusion of the current states does not change the measurement model, the exclusion of the bias state removes this term from the heading

measurement. The new measurement model is

$$\begin{aligned}
 y_k = h(x_k, v_k) = & \left[ \begin{array}{c} \sqrt{(E - A_E)^2 + (N - A_N)^2 + (Z - A_Z)^2} + v_A \\ \sqrt{(E - B_E)^2 + (N - B_N)^2 + (Z - B_Z)^2} + v_B \\ \sqrt{(E - C_E)^2 + (N - C_N)^2 + (Z - C_Z)^2} + v_C \\ \sqrt{(E - D_E)^2 + (N - D_N)^2 + (Z - D_Z)^2} + v_D \\ s + v_{s_m} \\ \Psi + v_{\psi_m} \end{array} \right]_k ; \\
 y = & \left[ r_A \quad r_B \quad r_C \quad r_D \quad s_m \quad \Psi_m \right]^T ; \\
 v = & \left[ v_A \quad v_B \quad v_C \quad v_D \quad v_{s_m} \quad v_{\psi_m} \right]^T .
 \end{aligned} \tag{2.19}$$

With the inclusion of the current estimates, this EKF should be able to accurately estimate the AUV state even when changing directions in current as this estimate uses a global frame of reference.

## 2.6 EKF Covariance Matrices

An important consideration when implementing any EKF is the interplay between the various covariance matrices. In an ideal case, accurate data would be available for statistical analysis of the true noise covariance for each state propagation, measurement and state estimate, allowing for a direct use of these values in the corresponding matrices. As this is generally not feasible, estimated error bounds can be used as a starting point and the values can be adjusted for beneficial filter behavior (e.g., the rate of convergence or robust stability). For simplicity, the process,  $Q$ , and measurement,  $R$ , noise covariance matrices are assumed to be constant with respect to time. Therefore the subscripts on these matrices are dropped.



### 2.6.1 Process Noise Covariance Matrix

The process noise covariances are a measure of the inaccuracies and variances of the propagation model in the EKF. These inaccuracies come from various sources, including discrete time step approximation, numerical integration order and unmodeled dynamics. The actual inaccuracies introduced into the propagation model are difficult to quantify and are thus estimated. These estimations were made based on typical errors bounds associated with the various approximations. The noise of the propagation of each state is assumed to be uncorrelated and thus the process noise covariance takes the form of a diagonal matrix. Of particular interest is the standard deviation associated with the east and north currents. The relatively small value of 0.001m/s indicates that the encountered currents are expected to remain fairly constant in the time scales considered. The process noise covariance matrix is given as

$$Q = \begin{bmatrix} \sigma_{wE}^2 & 0 & 0 & 0 & 0 & 0 \\ 0 & \sigma_{wN}^2 & 0 & 0 & 0 & 0 \\ 0 & 0 & \sigma_{w_s}^2 & 0 & 0 & 0 \\ 0 & 0 & 0 & \sigma_{w_\psi}^2 & 0 & 0 \\ 0 & 0 & 0 & 0 & \sigma_{w_{cE}}^2 & 0 \\ 0 & 0 & 0 & 0 & 0 & \sigma_{w_{cN}}^2 \end{bmatrix}; \quad (2.20)$$

with

$$\sigma_{wE} = 0.1\text{m};$$

$$\sigma_{wN} = 0.1\text{m};$$

$$\sigma_{w_s} = 0.01\text{m/s};$$

$$\sigma_{w_\psi} = 5^\circ;$$

$$\sigma_{w_{cE}} = 0.001\text{m/s};$$

$$\sigma_{w_{cN}} = 0.001\text{m/s}.$$

### 2.6.2 Measurement Noise Covariance Matrix

The measurement noise covariance matrix contains the noise associated with each measurement update to the EKF. As with the process noise covariance matrix, the measurements are assumed to be uncorrelated and thus this matrix also takes a diagonal form. The values used for the covariance of each measurement were estimated using collected data from previous field tests. More detail on how these covariances were estimated is provided below. The final form of this covariance matrix is

$$R = \begin{bmatrix} \sigma_{v_A}^2 & 0 & 0 & 0 & 0 & 0 \\ 0 & \sigma_{v_B}^2 & 0 & 0 & 0 & 0 \\ 0 & 0 & \sigma_{v_C}^2 & 0 & 0 & 0 \\ 0 & 0 & 0 & \sigma_{v_D}^2 & 0 & 0 \\ 0 & 0 & 0 & 0 & \sigma_{v_{sm}}^2 & 0 \\ 0 & 0 & 0 & 0 & 0 & \sigma_{v_{\psi_m}}^2 \end{bmatrix}; \quad (2.21)$$

with

$$\sigma_{v_A} = 3.3\text{m};$$

$$\sigma_{v_B} = 3.3\text{m};$$

$$\sigma_{v_C} = 3.3\text{m};$$

$$\sigma_{v_D} = 3.3\text{m};$$

$$\sigma_{v_{sm}} = 0.16\text{m/s};$$

$$\sigma_{v_{\psi_m}} = 5.75^\circ.$$

The measurement noise associated with the LBL ranges was assumed to be consistent between all the transponders, and all range magnitudes. This simplification may have some effect on the accuracy of the filter, but should be minimal as the majority of the noise on the

ranges is expected to be from the assumption that the speed of sound in water is constant across the entire operational space. Using data from previous field tests, an optimized position was determined for each set of ranges. This set of ranges is all the ranges collected from one acoustic navigation ping. Utilizing the topside tracking algorithm detailed in [22], an optimized position that minimizes the total error of the received ranges was solved for. This was used as a true position and the error of each range was determined. After analyzing various field test data, the standard deviation was estimated and used as the value for  $\sigma_A$ - $\sigma_D$ .

The speed of the AUV is estimated by a propeller RPM correlation. This correlation was obtained through empirical testing at various RPM values and was fit with a linear approximation. This speed estimate is treated as planar and thus is an inadequate estimate of the AUV speed when changing depths. Although there will generally be some out of plane speed at semi-steady-state depth, the planar speed should be fairly close to the RPM correlation as the empirical data would likewise have similar out of plane speed. As this correlation was taken from a relatively straight section of a mission, it may also be insufficient during cornering. By using a topside tracking range, an estimate of the variance on speed was obtained.

To get an estimate of the variance on heading measurement, recorded data from various field tests was analyzed. By looking at a straight portion of a mission, the variance on the heading was determined. This variance likely includes both the actual noise on the heading measurement, as well as any oscillations in the true heading. As with the covariance on speed measurement, this estimation was taken from a relatively straight section of a mission and thus may not accurately represent the variance during cornering.

### 2.6.3 State Covariance Matrix

The state covariance matrix,  $P$ , is an important aspect of the EKF. This matrix is continually updated during the recursion and is an estimate of the error associated with the current state estimation. This matrix is populated at the initialization of the EKF with the

square of the estimated error bounds associated with the initialization of each state. The initial position values,  $E$  and  $N$ , are established based on the GPS position mapped into local coordinates. Therefore the covariance on these states is initialized with an estimate of the variance associated with the GPS position. Although the speed and heading are fairly accurate when initialized, the dive sequence significantly perturbs these values, thus the covariances associated with these states are initialized higher to account for the unmodeled dynamics experienced during the dive sequence. This allows the states to vary more during the dive sequence, as the measured values may be insufficient estimates. An interesting covariance initialization in this matrix is the values associated with the currents. As mentioned above, the currents are expected to be slow changing, yet as there is no real-time information available to the AUV, the EKF is initialized with  $c_E = c_N = 0$  m/s. The covariance associated with these states is initialized correspondingly high. This high initial covariance is a way of accounting for the lack of knowledge of the state. This high initial covariance causes the estimate of these states to be highly transient until enough position measurements are accumulated and the estimation converges. This is seen as the values in the  $P$  matrix stabilize and lower. During this time, the state estimation is transient. Once converged, the EKF remains stable. More detail will be discussed on this in the results. The state covariance matrix is initialized as

$$P_0^+ = \begin{bmatrix} \sigma_{\hat{E}_0^+}^2 & 0 & 0 & 0 & 0 & 0 \\ 0 & \sigma_{\hat{N}_0^+}^2 & 0 & 0 & 0 & 0 \\ 0 & 0 & \sigma_{\hat{s}_0^+}^2 & 0 & 0 & 0 \\ 0 & 0 & 0 & \sigma_{\hat{\psi}_0^+}^2 & 0 & 0 \\ 0 & 0 & 0 & 0 & \sigma_{\hat{c}_{E0}^+}^2 & 0 \\ 0 & 0 & 0 & 0 & 0 & \sigma_{\hat{c}_{N0}^+}^2 \end{bmatrix}; \quad (2.22)$$

with

$$\sigma_{\hat{E}_0^+} = 5\text{m};$$

$$\sigma_{\hat{N}_0^+} = 5\text{m};$$

$$\sigma_{\hat{s}_0^+} = 1.5\text{m/s};$$

$$\sigma_{\hat{\psi}_0^+} = 20^\circ;$$

$$\sigma_{\hat{c}_{E0}^+} = 1\text{m/s};$$

$$\sigma_{\hat{c}_{N0}^+} = 1\text{m/s}.$$

## 2.7 MOOS Heading Controller

For navigation, the UI AUVs follow a set of predefined waypoints. For more precise navigation, it is desired that the AUVs stay on the path directly connecting the previous and next waypoints. To accomplish this, a heading controller was designed based on the Mission Oriented Operating Suite (MOOS) track-line following behavior [1].

The MOOS track-line following behavior utilizes the waypoint positions, the AUV's estimated position and a look-ahead distance to calculate a desired heading for the AUV. Specifically, the desired heading is found by calculating vectors both from the previous waypoint and the AUV to the next waypoint; these are referred to as the path and target, respectively. These can be seen in Figure 2.3. Using the look-ahead distance and vector algebra, a ghost waypoint is placed on the path ahead of the AUV and the vector from the AUV to this waypoint is calculated. The heading of this vector is set as the desired heading and the heading error is found and passed to a proportional feedback heading controller.

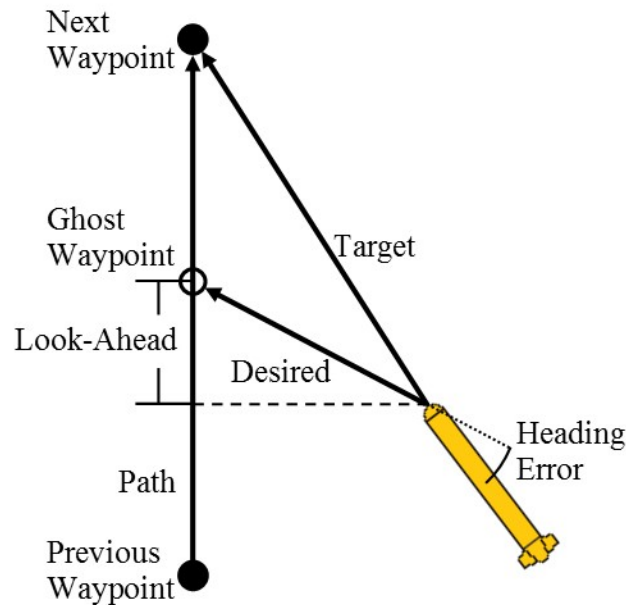


**Figure 2.3:** The MOOS heading control uses a predefined look-ahead distance to set a desired heading.

This calculation is repeated at every time step, with the ghost waypoint always along the path ahead of the AUV by the look-ahead distance. As the AUV approaches the line, the desired heading to the ghost waypoint asymptotically approaches the direction of the waypoint path. This creates a damped response (the AUV tracks to the desired path without overshoot) in the ideal case. As the AUV position is taken from the EKF estimate, the effectiveness of the MOOS heading controller is dependent on an accurate EKF estimate. Thus, accurate position estimation is paramount.

## 2.8 Modified MOOS Heading Controller

When operations are extended to oceanic environments, the MOOS heading controller may be insufficient as any side current will keep the AUV from following the desired path. To improve the MOOS heading controller, the estimated currents can be leveraged with knowledge of the relationship between velocity through water (VTW) and velocity over ground (VOG), as

explained earlier. Using the estimated currents and equating the VOG to the previous MOOS heading vector, a VTW can be determined which accounts for the effect of current.

To fully achieve this, the controller would need two degrees of freedom; speed and heading. As the specific location along the waypoint path is not as important as converging to the path, the parallel-to-path current can be neglected. With this simplification only one degree of freedom is required; heading. This is desired as the AUV has a fairly narrow band on the RPM values that will allow the AUV to remain at the set depth and under control. Using relative magnitudes and geometric relationships, a compensated heading is calculated that compensates for the estimated currents. For a detailed derivation, see Appendix B.

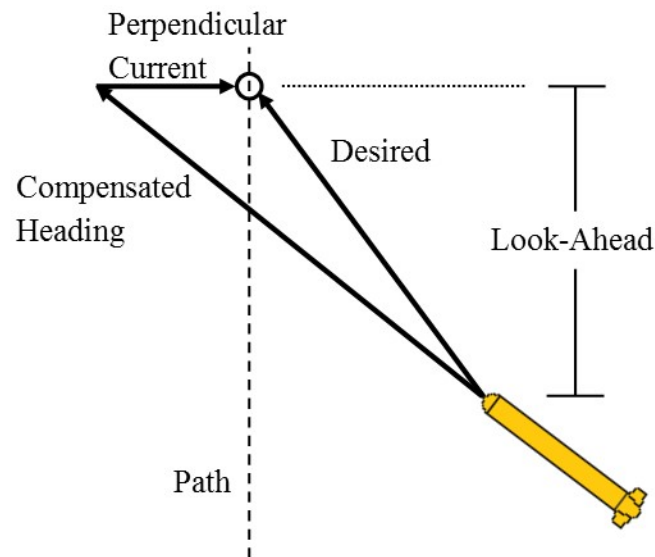


**Figure 2.4:** The modified MOOS heading controller uses the estimate of perpendicular to path current to establish a new desired heading that will drive the AUV onto the waypoint path in the presence of currents.

Figure 2.4 shows the modified MOOS heading controller that compensates for the estimated current. As stated above the parallel-to-path current is neglected in this calculation, thus the position that is actually navigated towards may be shifted along the waypoint path based on

this current. Important to the calculations is that the magnitude of the perpendicular-to-path current is less than the relative speed of the AUV. As the AUV cannot operate effectively in currents higher than its operational speed, this is a scenario that should only be encountered with a bad estimation. As this is possible during the initial convergence of the EKF, the software implementation includes a check of whether or not the magnitude of the estimated current is larger than that of the VTW. If so, the original MOOS heading control will be used until a valid current estimation is achieved. As this should only occur with a bad estimation, navigation will already be degraded and thus the lack of convergence associated with this controller is of no consequence.

## 2.9 Estimation and Navigation Simulations

To evaluate the effectiveness of the adaptations made for ocean currents, simulations were conducted in Matlab. These simulations were conducted and compared for the previous EKF, new EKF, and new EKF with modified controller. The basis for comparison was twofold; first, the error between the EKF estimate and the true state; second, the off-path error. As the new EKF is meant to replace the previous EKF in all operations, it is desired that it have comparable or improved accuracy in all possible encountered currents, including the zero current case.

As it is desired that the simulation be as comparable with field testing as possible, it uses realistic measurement noises, calculated from field testing data in the same manner as for the covariance matrices detailed above. To further keep the simulation realistic, the EKF is initialized with a noisy state, similar to what is expected in field testing. To keep the simulation unbiased amongst the various EKF and MOOS controller permutations the noise was seeded the same, thus being held the same across the various simulation cases.

For the simulations a course of  $100 \times 50\text{m}$  was chosen. As stated above, it is desired that the new EKF work comparably or better than the previous EKF. The first simulation was a zero current case, which is the case that the previous EKF was designed and optimized for. This is important as it is the best comparison between the new and previous EKF accuracies. Next, the



simulation was expanded to include a constant current. For this simulation case, the current was set to have components of  $-0.15$  m/s in the east direction and  $0.4$  m/s in the north direction. With both of these simulation cases all three permutations were simulated and compared for the criteria stated above.

## **2.10 Estimation and Navigation Field Testing**

To prove the effectiveness of the various changes, field testing was conducted at the Office of Naval Research's (ONR) Acoustic Research Detachment (ARD) in Bayview, ID. This facility is located on Lake Pend Orielle and is equipped with a bottom mounted acoustic tracking array to provide an independent estimate of the AUV's position as it navigates. This tracking system is an improved version of the tracking system detailed in [22]. This allows for a comparison of the on-board EKF estimate with a secondary estimate.

A long baseline (LBL) array of Hydroid transponders, anchored on the day, is utilized for acoustic ranging. These transponders are surveyed and calibrated before testing commences. To mitigate errors introduced with assumptions such as constant speed of sound across the operational area, the transponders are placed outside the operational area. This LBL array provides the position measurements for the EKF.

With the use of the acoustic tracking range, the EKF estimated position was compared to the acoustic tracking system solutions. As the tracking solutions are a discrete position estimate, only available when the AUV transmits a navigation ping, the comparison can only be made at these points. Assuming the acoustic tracking system to be highly accurate, this position is held as the true position. Calculating the error of the EKF estimate against the acoustic tracking position estimate gives a basis for comparison of the various tests. As the depth of the AUV is assumed known, only the planar position discrepancy is considered.

### 2.10.1 Zero Current

The first field test with the new EKF was a verification test in a low current environment. The purpose of this test was to ensure that the EKF was implemented correctly and behaves as expected. Additionally, this tests that the modified MOOS heading controller navigates accurately with a low current estimation.

As the water at the ARD testing range is very slow moving, save for wind effects on the surface, the EKF, if working correctly, would estimate little to no current, and remain stable apart from the initial transient period at the mission start. Though the exact water currents are not known the magnitude of these currents are expected to be negligible, well below the expected accuracy of the EKF. The effectiveness of the new EKF was evaluated by comparing the accuracy of the EKF estimate in these field tests to previous published work.

### 2.10.2 Simulated Current

A second field test scenario was conducted with a simulated current. As it is difficult to induce a stable forced current across the operational area this simulated current was induced in software. To achieved this the EKF was modified to include known constant biases,  $c_{ESIM}$  and  $c_{NSIM}$ , in the propagation matrix as shown in

$$\begin{bmatrix} E \\ N \\ s \\ \psi \\ c_E \\ c_N \end{bmatrix}_{k+1} = \begin{bmatrix} E + s \sin \psi \Delta t + c_E \Delta t - c_{ESIM} \Delta t + w_E \\ N + s \cos \psi \Delta t + c_E \Delta t - c_{NSIM} \Delta t + w_N \\ s + w_s \\ \psi + \dot{\psi} \Delta t + w_\psi \\ c_E + w_{c_E} \\ c_N + w_{c_N} \end{bmatrix}_k. \quad (2.23)$$

These biases create a position discrepancy between the EKF estimate and the measured position, the same magnitude as a constant current with the components of the biases would

produce. For convenience the bias terms were included as negative terms so as to produce a positive EKF estimate of the simulated currents.

With the modified MOOS controller implemented along with this simulated current, a predictable offset from the waypoint path can be calculated that the AUV should converge towards. This is due to the MOOS heading controller attempting to compensate for an estimated current that does not physically exist. Comparing the EKF estimate and associated acoustic track to the theoretical offset gives a test of the behavior of the modified MOOS heading controller.

## Chapter 3: Results & Discussion

### 3.1 AUV Control Gains Testing

The control gains were altered to achieve more stable operations at higher speeds while maintaining the stability at lower speeds. To this end, the effectiveness of the various gains were compared based on the frequency and amplitude of oscillation during steady-state operations. Ideally there would be no oscillation, which is advantageous for the processing of scientific measurements, yet in practical implementation this is rarely possible.

#### 3.1.1 Simulation

As stated above, the control gains were simulated at higher speeds with various permutations of proportional gains. As the simulation uses a simplified geometry, the predicted frequencies and amplitudes of oscillations were not inherently useful. Yet, comparison of these attributes indicated the direction to perturb the gains for beneficial behavior. As the simulation is uncoupled, the heading was considered separately from the pitch and depth.

For pitch and depth control, the control issue is convoluted by the fact that both states are controlled by a single degree-of-freedom. Thus the interplay between the gains is exceedingly important. To investigate the trends associated with this interplay, a parametric study was conducted. The standard depth and pitch gains were used as well as double and half of each of these values. As the depth and pitch are highly coupled, stability with regards to one implies stability with regards to the other. Due to this, only the depth output was evaluated to determine the effectiveness of the gain set.

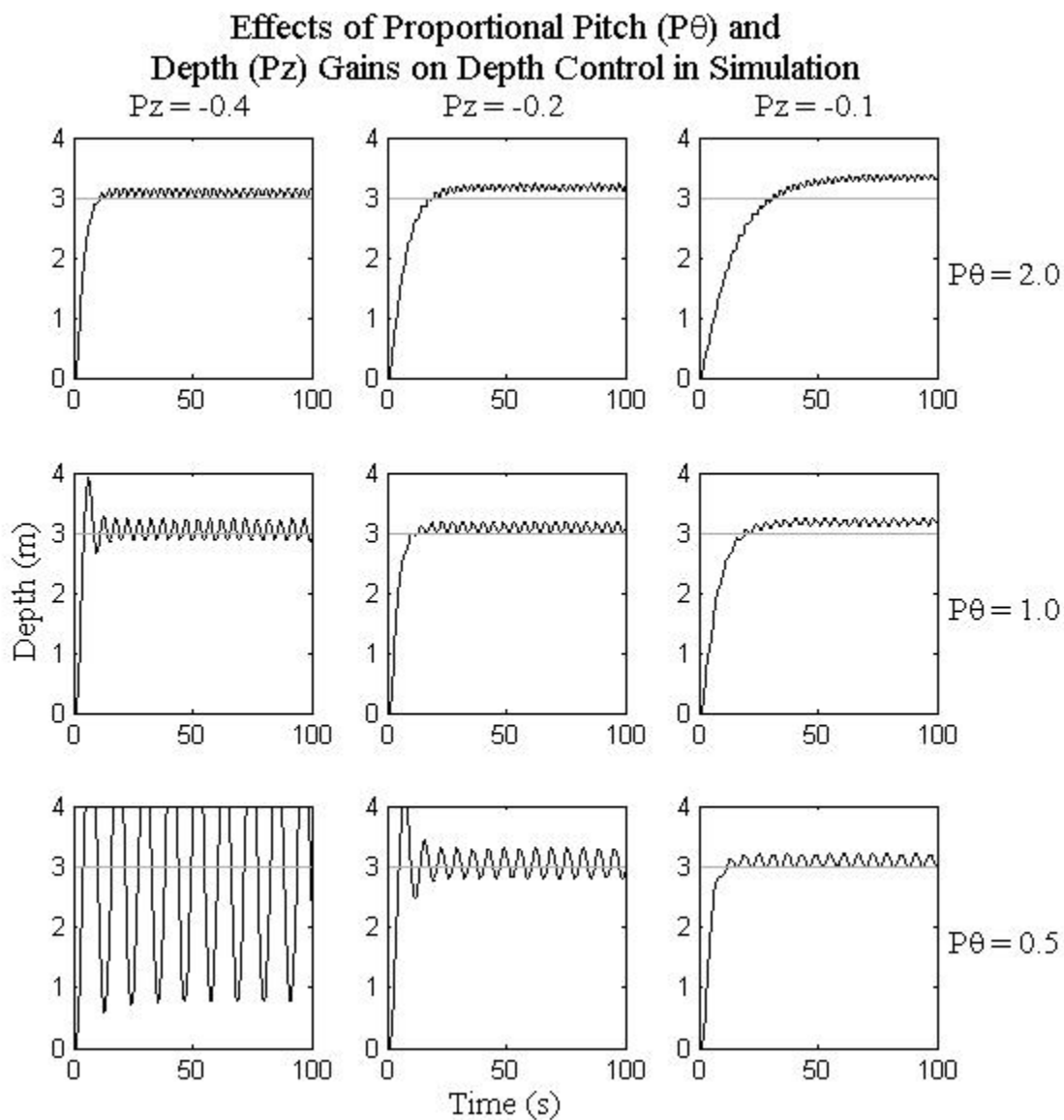


**Figure 3.1:** Proportional pitch,  $P_\theta$ , and depth,  $P_z$ , gains parametric study simulation output.

From Figure 3.1 it can be seen that both proportional gains have a significant effect on the oscillation of the depth, and thus on the pitch. Also noted is the effect of the proportional gains on the time it takes to reach the specified depth. In addition to this, as can be seen clearly in the top right graph of Figure 3.1, the simulation predicts a slight steady-state offset from the set depth. As the depth is recorded during the AUV missions, a slight offset from the set depth is acceptable as long as it remains close.

By analyzing the trends associated with the various gain combinations, the sets of gains associated with the top right 4 plots in Figure 3.1 were selected as viable options for field testing. These were selected as they had the smallest amplitudes of oscillation. Additionally, as previous field tests have shown a high tendency of the AUV to overshoot the desired depth, the slower approach to depth could be beneficial.

For the heading control, only one gain controls the response in the simulation. In application, this would only be the case if the AUV did not roll. As it has been observed that the AUV does roll during operation, this simulation will not capture the true dynamic effects of the control gains. Yet, this simulation is still useful for evaluating the trends associated with the heading gain. Like with the depth and pitch gains, values of double and half the previous standard were used to establish the trends. Likewise, the amplitude and frequency of oscillation were used to determine the beneficial behavior. Figure 3.2 shows the simulation outputs of the various gain values analyzed.

### Effect of Proportional Heading ( $P\psi$ ) Gain on Heading Control in Simulation

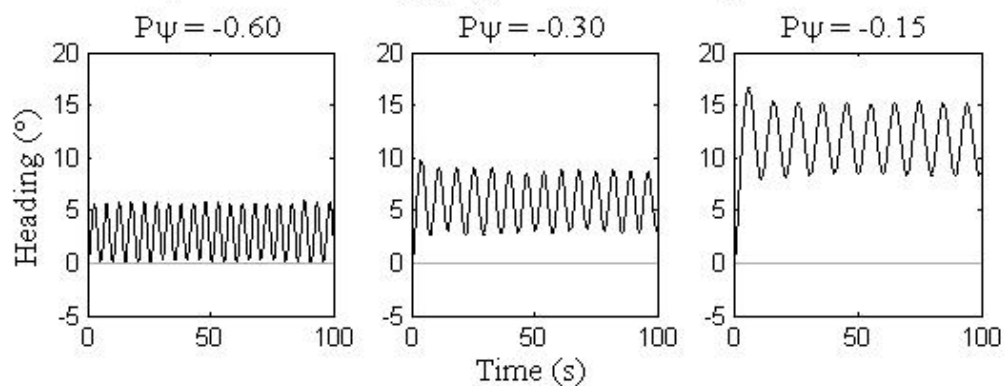


**Figure 3.2:** Proportional heading gain,  $P\psi$ , simulation output.

From this simulation it can be seen that the simulation predicts a smaller amplitude of oscillation with the higher proportional gain on heading. Also, similarly to the pitch and depth, the frequency goes up with the smaller amplitude. An interesting peculiarity noticed with this simulation is the mean value of the heading. The target path was set to due north, or  $0^\circ$ , yet all the simulations were offset from this; the lower the gain, the larger the offset. The reason for this offset was not apparent, and would likely require re-derivation of the control laws and a detailed check of the simulation implementation to determine the cause. Regardless of this peculiarity, the simulation output was used to select gains to implement on the AUV for field testing.

For implementation of heading gains for field testing, the higher gain,  $P\psi = -0.60$ , was used along with the standard gain,  $P\psi = -0.30$ . Similarly to the depth and pitch gains this was aimed at minimizing the amplitude of oscillation. Although the higher frequency of oscillation is not desirable, having the smaller amplitude oscillations is of more importance.

### 3.1.2 Field Testing

As any changes to the control gains are only useful if they work in implementation on the AUV, it was desired to validate the simulation results with field testing. When conducting the field testing, the control issue is convoluted by the roll of the AUV. As the roll is not accounted for, any attempt to change pitch or depth while the AUV is rolled, even slightly, will perturb the heading, and vice versa. Thus the effects of the proportional gains may not be as obvious as they were in the simulation data. To test the effectiveness of the gain changes, the previous standard gains were used as a baseline. These field tests were conducted at various mission RPMs to evaluate the performance across much of the operational range. As there was no independent measure, the AUV recorded data was used to assess performance.

As stated, four permutations of gain values were evaluated as viable options. These correspond to the top right four plots in Figure 3.1. This includes the previous standard, which was used as a basis for comparison. All permutations of gains were tested at 3 RPM values,

which span much of the operational range. These values were 800, 1000, and 1500 RPM.

### Effects of Proportional Pitch ( $P\theta$ ) and Depth ( $Pz$ ) Gains on Depth Control in Field Testing

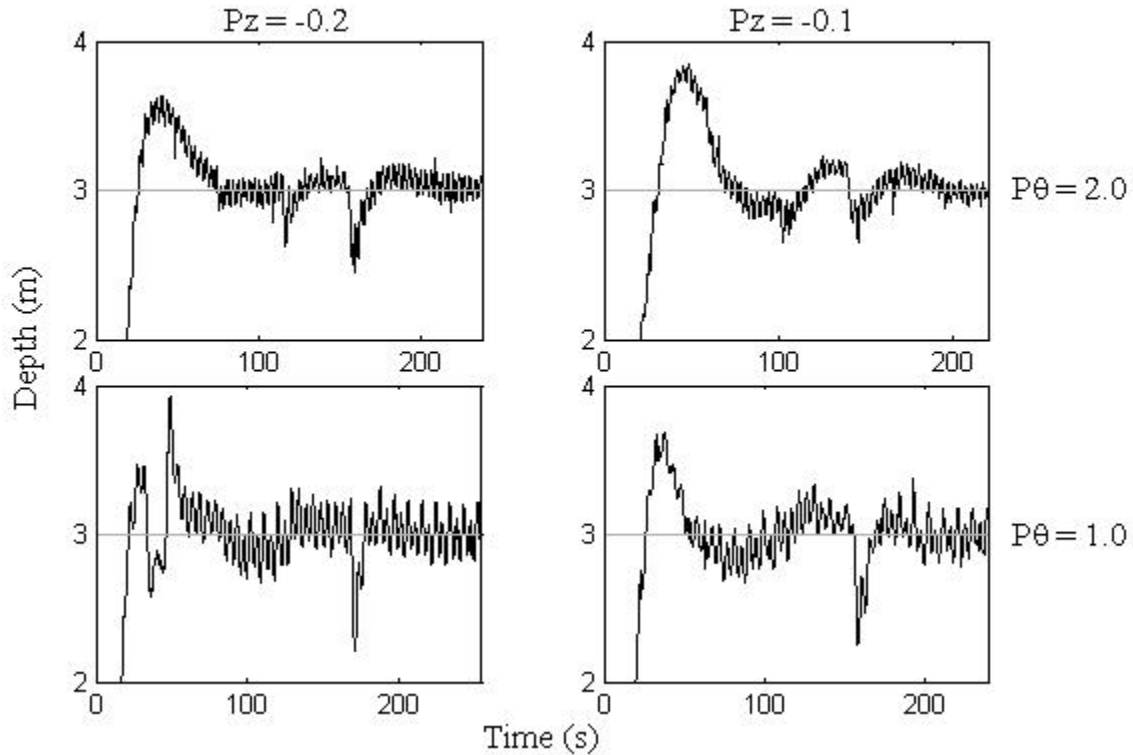


**Figure 3.3:** Proportional pitch,  $P\theta$  and depth,  $Pz$ , gains parametric study field testing at 1500 RPM.

Shown in Figure 3.3 is the AUV recorded depth during the 1500 RPM missions. As all gain sets resulted in similar performance at the 800 and 1000 RPM operations, the analysis focused on the 1500 RPM missions. As can be clearly seen the field test results follow a similar trend to that predicted by the simulation. Table 3.1 shows the root-mean-squared (RMS) depth errors during a steady-state section around 100 seconds into the mission.

**Table 3.1:** Effect of proportional pitch,  $P\theta$ , and depth,  $Pz$ , gains on depth oscillations in field testing. Given values are root-mean-squared (RMS) depth error.

	$Pz=-0.2$	$Pz=-0.1$
$P\theta=2.0$	0.0593m	0.0565m
$P\theta=1.0$	0.1281m	0.1172m

From Figure 3.3 and Table 3.1 it is clear that the gains set with  $Pz = -0.1$  and  $P\theta = 2.0$



improve the performance of the depth and pitch control. The results presented here follow the same trends as those from AUVs with different external sensors. With these results, the standard operational gains have been changed to take advantage of this improved performance during higher speed operations.

In a separate field test from the pitch and depth gains parametric study, the heading gain was analyzed. This followed a similar procedure as that of the pitch and depth test, evaluating the selected gain against the standard gain across various RPM values. Again, the recorded data from the AUV was used to compare the effectiveness of the gain change. Similarly to the pitch and depth, the heading was relatively stable for the lower RPM missions. Therefore, the 1500 RPM mission was used to evaluate the performance. Figure 3.4 shows the recorded heading for these missions.

#### Effect of Proportional Heading ( $P\psi$ ) Gain on Heading Control in Field Testing

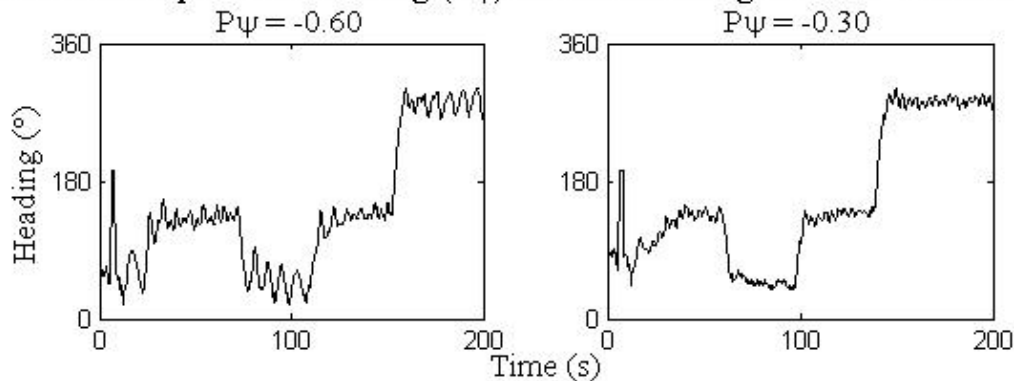


**Figure 3.4:** Proportional heading gain,  $P\psi$ , field testing at 1500 RPM.

As can be clearly seen in Figure 3.4, the field test results do not agree with the simulation prediction. The gain predicted by the simulation to lower the amplitude of oscillation actually increased the amplitude over what is seen with the previous standard gain. This is corroborated by the RMS values in Table 3.2.

This false prediction, along with the peculiarities mentioned above, point to an error in the heading calculation of the simulation. There may be some interaction with the MOOS heading controller that is not implemented in the simulation, though this is not expected to significantly impact the oscillations. As these gains should not need to be evaluated again unless

**Table 3.2:** Comparison of the RMS heading error during steady-state field testing between the standard and simulation predicted gain.

	$P\psi=-0.6$	$P\psi=-0.3$
RMS Heading Error	11.94°	4.94°

a major change is made to the AUVs, a re-derivation of the control laws to fix the heading simulation is not worthwhile. Efforts to investigate a more robust and accurate model of the AUV with realistic geometry utilizing computational fluid dynamics (CFD) are underway. This CFD model may be leveraged to create a more accurate control simulation. More detail on this will be provided in the next chapter.

Although the field test suggested that improved performance could be achieved by tuning the gain the opposite way than the simulation predicted, the standard gain is being retained. This is due to the observed trend of lower amplitude being coupled with higher frequency oscillations. As the standard gain works fairly well, with neither high amplitude nor high frequency oscillations, it was deemed sufficient for AUV operations.

### 3.2 Chained-Missions Continuous EKF Field Test

To validate that the chained mission continuous EKF was working as desired, field testing was conducted at the Navy's Acoustic Research Detachment (ARD). Various mission types were chained together in differing orders to ensure that the continuous EKF propagated correctly for any set of chained mission. Although many of the missions were conducted on the surface it was desired that the EKF not re-initialize with GPS position as there is no guarantee that the AUV will be on the surface between missions, and adding logic to check for this would over-complicate the implementation.

For the test shown in Figure 3.5, the first mission was an underwater timed mission with a set heading of 135°; this was followed by a 0 RPM timed mission to allow the AUV to float to the surface and establish a GPS position. Next, a GPS mission was utilized to stage the AUV. This was followed by an LBL mission and a subsequently another stage mission. The EKF

estimate during this series of missions is show in Figure 3.5 with the start of each mission denoted per the legend.

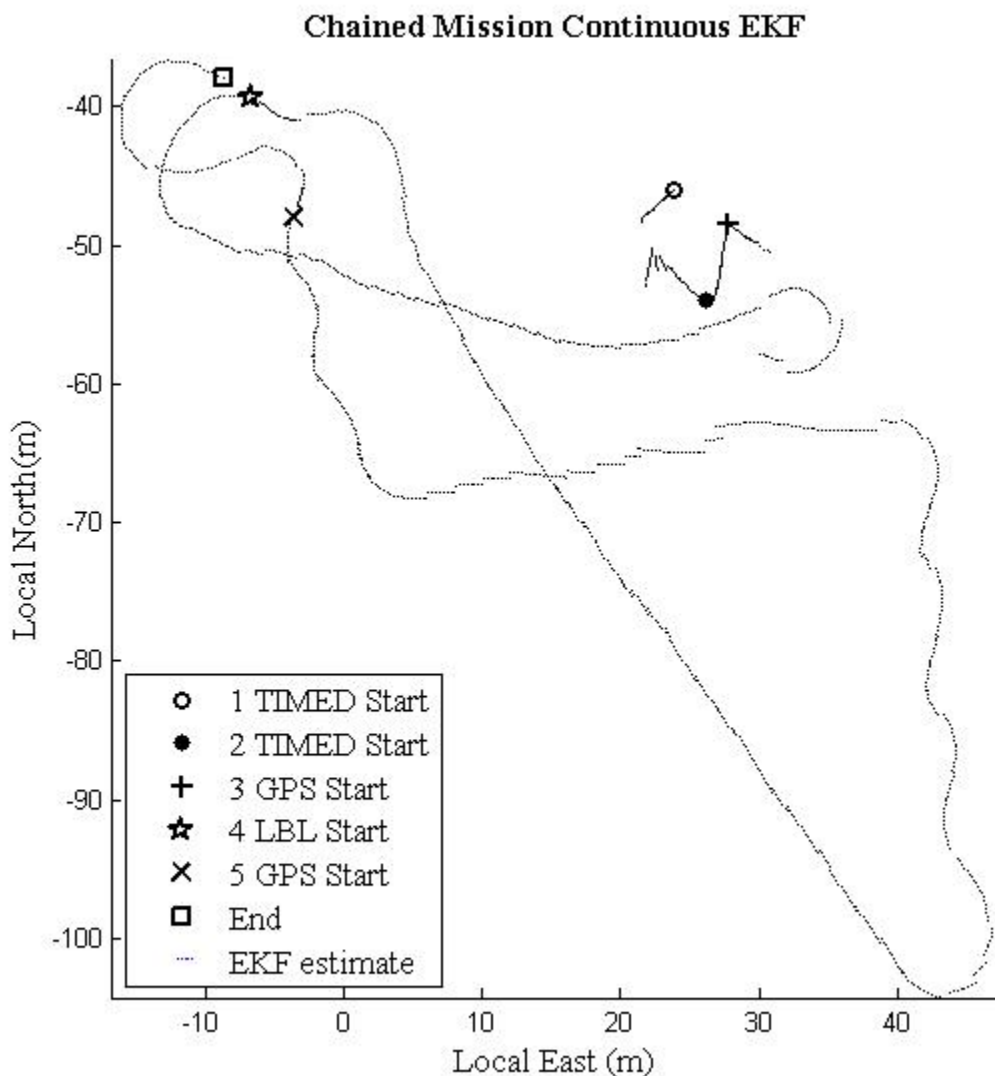


**Figure 3.5:** Continuous EKF estimate propagated throughout several different mission types for a set of chained missions.

With this test of the chained missions, some peculiarities were uncovered. The most notable of these is due to how the speed correlation was implemented in the AUV source code. This implementation is a linear regression between RPM and speed,  $s$ , in m/s based on field test data taken in the normal operating range of the AUV. As the EKF has not been propagated in either the GPS or timed missions previously, there was never a situation where the EKF was

propagated with an RPM outside of this operating range. As the linear relationship includes a negative offset, as shown in Equation (3.1), the EKF was fed a negative speed measurement during the 0 RPM timed mission.

$$s = 0.001138(RPM) - 0.2533 \quad (3.1)$$

In addition, this float up mission had no acoustic broadcasts, thus the EKF did not receive a position measurement. Without position measurements, the EKF becomes unobservable and the current estimates are not updated. This caused problems as the current estimates are transient for a significant amount of time after the EKF is initialized. Therefore, the currents were held fixed at the last estimate, which was not accurate, for the entirety of this second mission. The artifact of this problem with the speed correlation and stagnated current estimate can be seen in Figure 3.5 after the second mission starts, denoted by ●, where the EKF estimate abruptly heads northerly. Once the GPS mission is started, denoted by +, and an acoustic position measurement is acquired, the EKF estimate jumps back nearly collinear with the path it diverged from.

Another peculiarity with the EKF estimate, which is not unique to the chained missions, is how the speed measurement is handled during the dive sequence. When the AUV is propagating through the steps of the dive sequence, the speed measurement is hard-coded to .5 m/s. This may be a valid estimate of the speed during forward dives, but, as the reverse dive is more reliable, this dive has become the standard. With the reverse dive, the AUV reverses nearly vertically then starts to flatten out, before switching to forward motion. This entire sequence results in little planar motion and thus a constant forward speed is an insufficient estimate for this sequence.

Although there were some peculiarities uncovered with this field test of the chained missions EKF, the concept was shown to work. The EKF initializes on the first mission, regardless of type of mission. Additionally, it is updated correctly throughout all the missions

in the chained set. Although the 0 RPM mission in the set had a negative speed that wasn't corrected for, it is believed that this may be mitigated with the use of acoustic navigation pings. In the results shown in Figure 3.5 the 0 RPM mission was not set to use acoustic communications and thus there were no position updates during this time. Therefore, the EKF had no information to contradict the incorrect speed measurement due to the insufficient speed correlation, nor update the current estimates. As operations are generally only conducted between 800 and 1500 RPM, where the speed correlation is valid, the inadequacy of the speed correlation outside this range is of little importance. If operations are expected to include 0 RPM missions the speed correlation can be modified to include a deadband that will set the AUV speed to 0 m/s below a specified RPM value. As the purpose of this field test was to ensure a continuous EKF for chained missions that properly updated with measurements throughout all mission types, this field test was successful. Although only one chained set of missions is shown, several sets were carried out and analyzed. All of these showed proper initialization and update of the EKF throughout, regardless of what types of missions were included or the order of missions.

### **3.3 Estimation and Navigation Simulation Results**

The EKF simulations detailed in Chapter 2 were performed. The position error between the estimated and true state, as well as the off-path error are reported and compared in this section. As there is a five meter acceptance threshold on the waypoints the AUV switches to the next waypoint early creating a jump in the off-path error. As this is seen in all permutations of EKFs and MOOS controllers, this is not corrected for, but accounted for in analysis. Due to this inherent error, the mean off-path error is not used as a metric. Instead, a qualitative analysis is used to evaluate this performance. As for the estimation error, two values are reported; total average estimation error and steady-state average estimation error. Due to the covariance interactions early in the EKF estimation, there is an estimation error until the EKF stabilizes and converges. This convergence time is more significant for the new

EKF than the old EKF. Though the time to converge and associated error is important, the steady-state error is arguably more important.

### 3.3.1 Zero Current

The zero current test is important as it will be the most direct comparison of accuracy between the previous and new EKFs. As the previous EKF was designed and optimized for performance in this environment, it should provide the best accuracy with this EKF.

The simulation of the previous EKF, shown in Figure 3.6, shows quick convergence and relatively stable estimation. As the noise implemented in the simulation was based on the estimated noise values used for the covariance matrices in the new EKF, the simulation is likely slightly biased towards the new EKF. Additionally, this previous EKF was optimized against field test data and thus may account for some unmodeled effects. Regardless, the previous EKF is in the range of the accuracy achieved in previous field tests.

With the new EKF, the estimation is more stable. This can be seen in Figure 3.7. Although the accuracy is better than with the previous EKF, this may only be a manifestation of the simulation bias mentioned. One aspect to note with this new EKF is the slower convergence time. Due to how the current is estimated, it takes the EKF a significant amount of time to become stable and accurate. Although this takes time, once converged the estimation remains accurate, which is more desirable than quick convergence.

With the inclusion of the modified MOOS heading control in the zero current case the estimation and navigation is virtually unaffected. This is due to the modification to the MOOS heading controller converging to be equivalent to the unmodified MOOS heading controller if the current is estimated as 0 m/s. Due to the negligible estimated current, the navigation is very similar to that with the unmodified MOOS heading controller. Figure 3.8 shows the results of this simulation case.

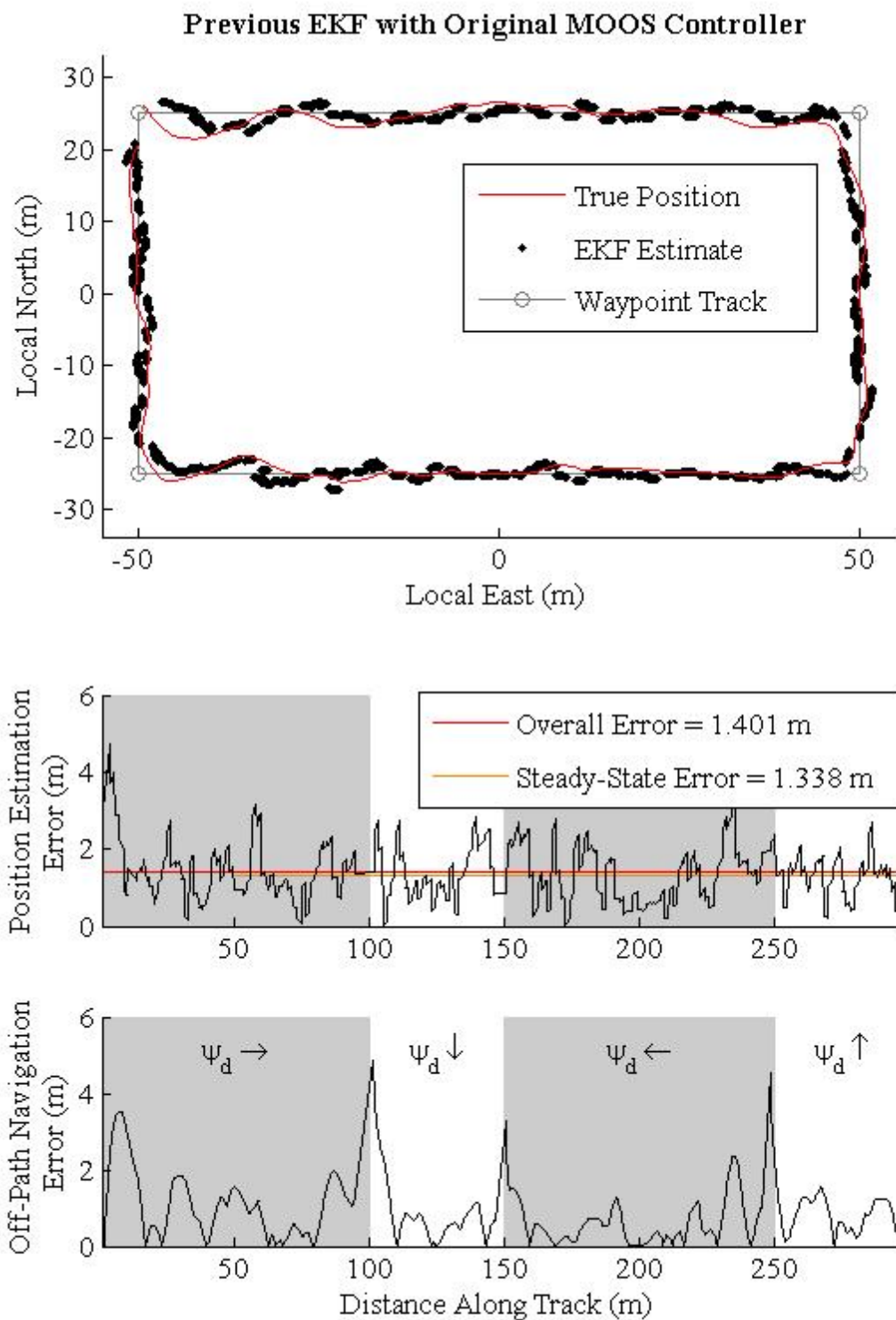


**Figure 3.6:** Previous EKF simulation in zero current.

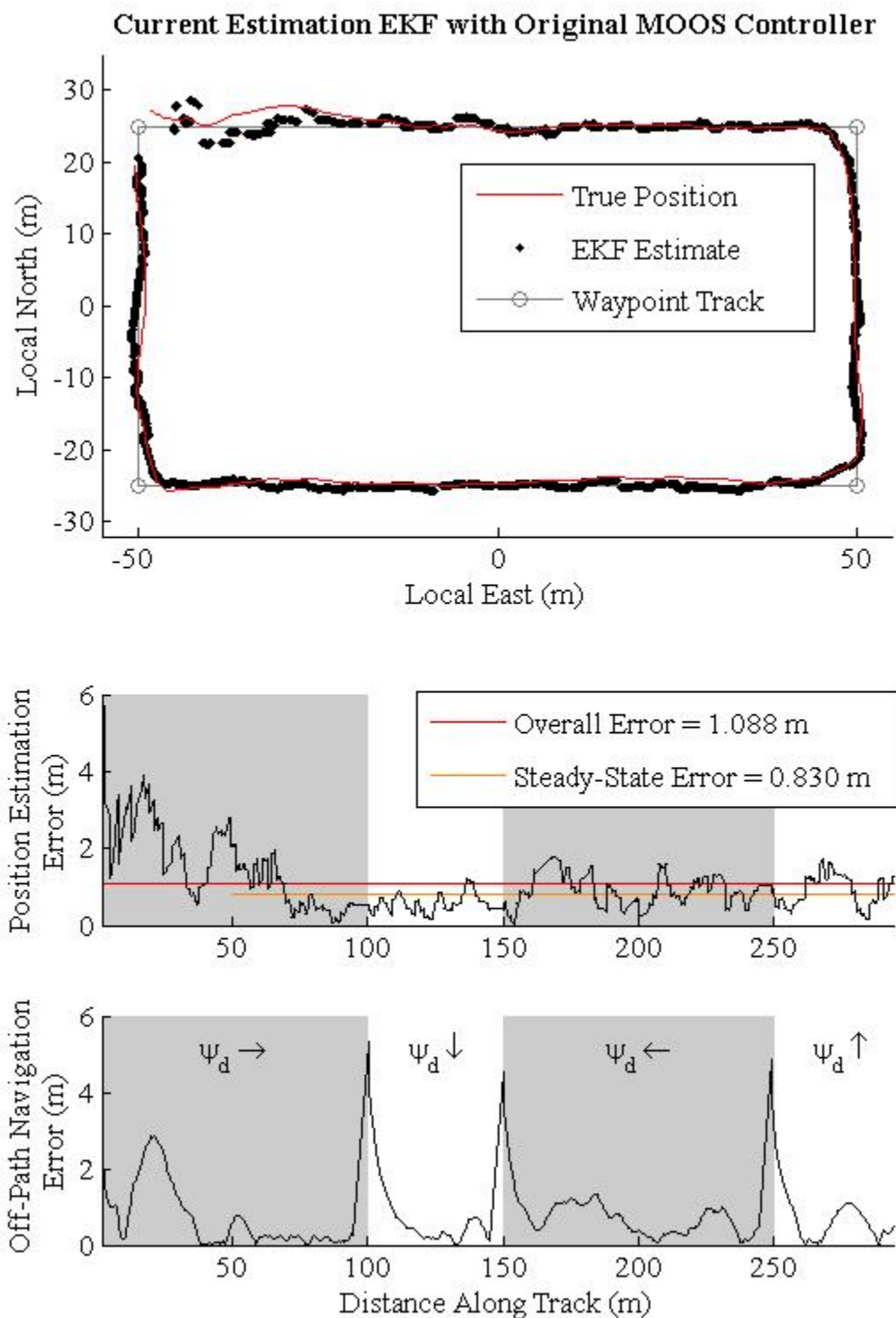


**Figure 3.7:** New EKF simulation in zero current.



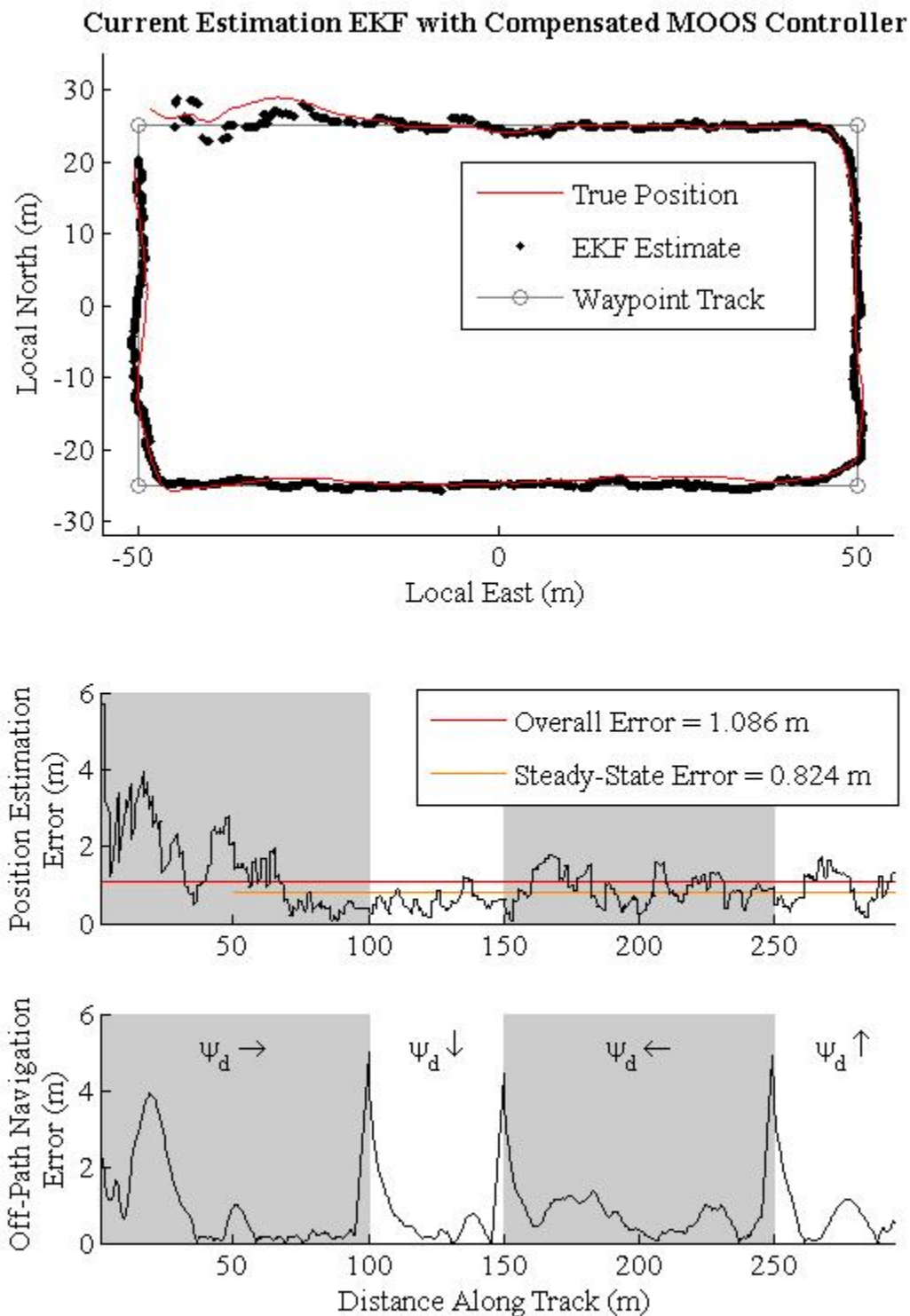


**Figure 3.8:** New EKF with modified MOOS controller simulation in zero current.

From Figures 3.6 to 3.8 it can be seen that there is a similar off-path error in the zero current case. As can be seen in all the simulation figures, there is a jump in the off-path navigation error when changing directions. This is produced by two sources: the acceptance threshold for the waypoints and limited turning radius of the AUV in simulation. Due to this large divergence, a qualitative analysis was used. As there is no current to affect the navigation, the off-path error will be correlated with the accuracy of estimation. One interesting aspect is that the previous EKF seems to jump around more, which can be seen in the off-path error changing more quickly. This seems to suggest that the previous EKF is trusting the accuracy of the ranges more, and reacting to any positional discrepancies. As the noise on the range measurements was estimated from a large ocean course, the noise may be higher than what the previous EKF was optimized for.

### 3.3.2 Constant Current

As stated earlier, the simulation was setup to include constant currents. To test the effectiveness of the new EKF in current, the simulation was conducted with a constant current of  $-0.15$  m/s in the east direction and  $0.4$  m/s in the north direction. For comparison, the previous EKF was also simulated in this constant current.

As can be seen in Figure 3.9, the previous EKF is able to correct for the constant current. This is captured by estimating a heading bias and a speed that differs from the RPM correlation. This works fairly well when traveling in one direction. The problem with this approach is that any change in direction will result in a transient time to find the appropriate biases for the new direction. This is due to the fact that these biases are in the AUV's frame of reference while the currents are in the global frame of reference. As such a more robust solution is desired.

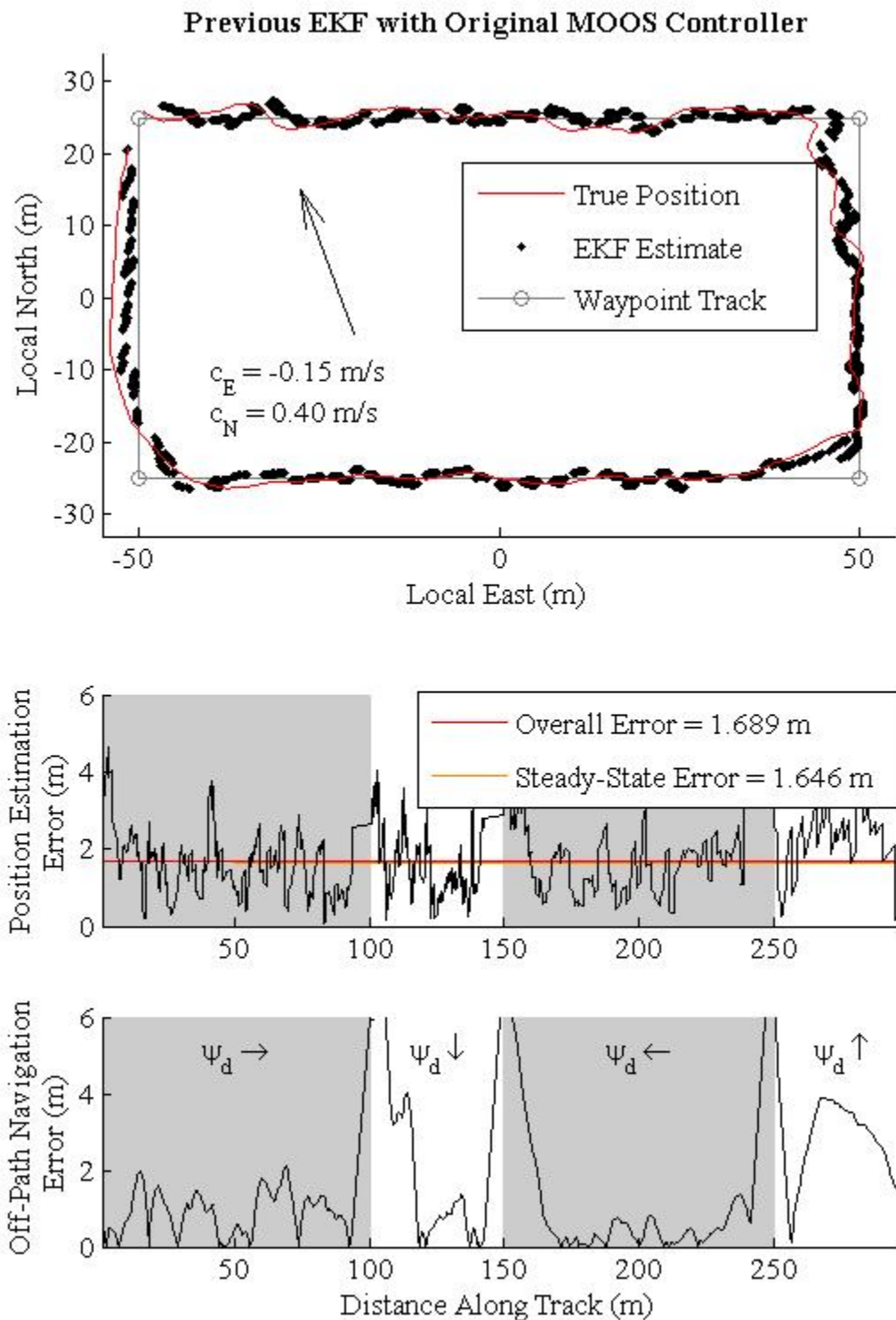


**Figure 3.9:** Previous EKF simulation in a constant current.

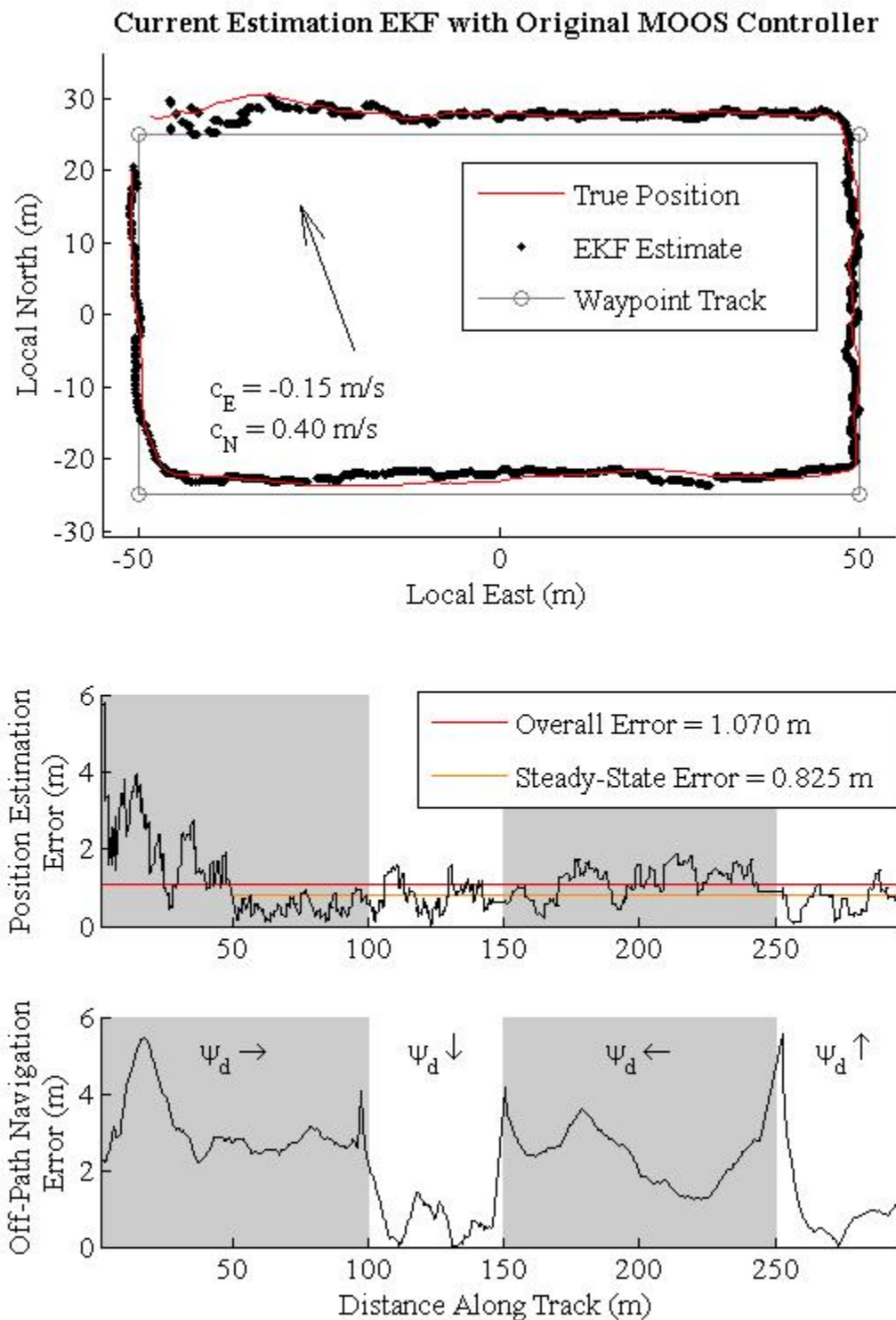


**Figure 3.10:** New EKF simulation in a constant current.

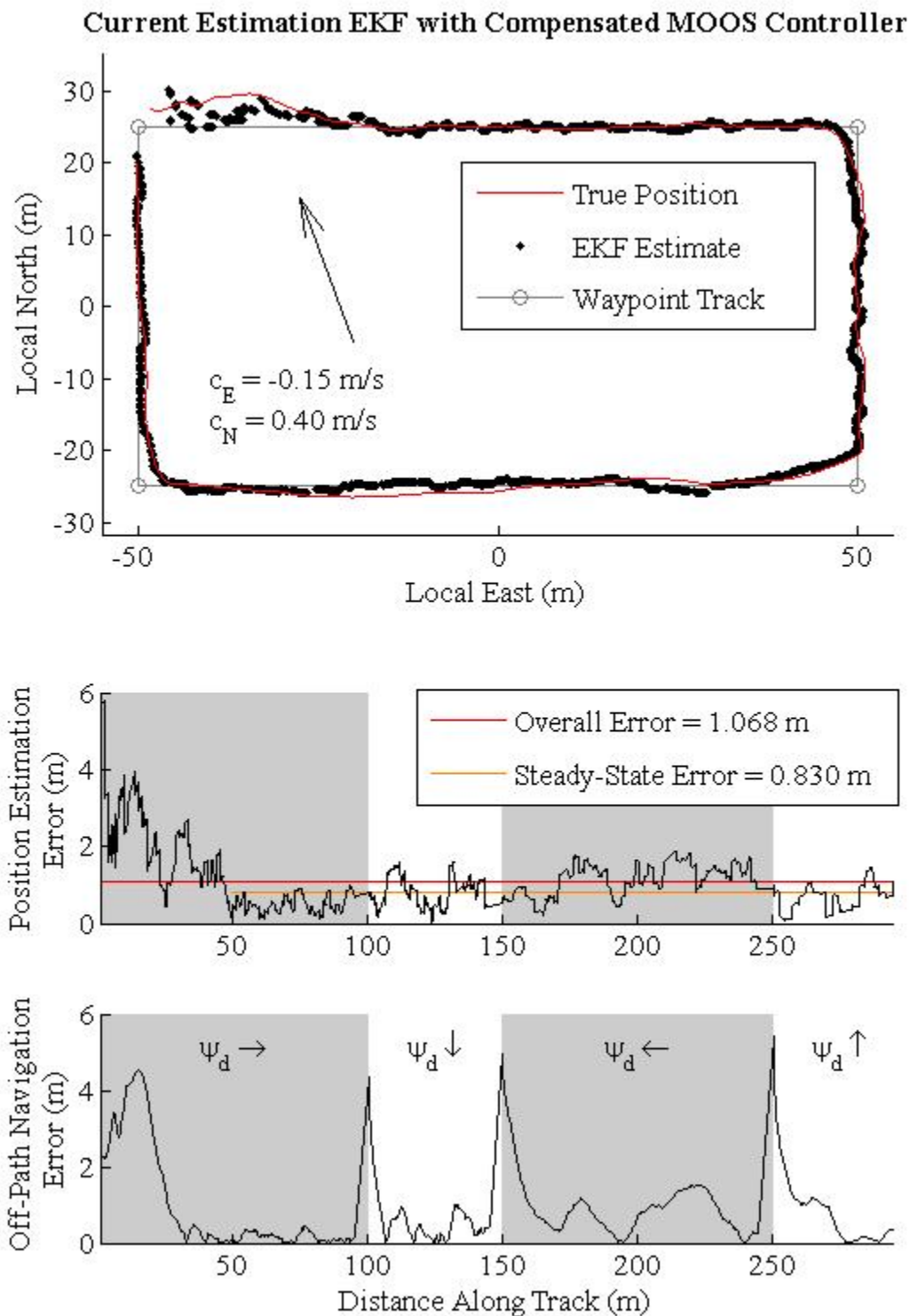


**Figure 3.11:** New EKF with modified MOOS controller simulation in zero current.

Due to this degraded estimation and navigation when changing directions using the previous EKF, the new EKF was designed to directly estimate the water currents and include these in the state calculations. This eliminates the transient when changing directions as can be seen in Figure 3.10. Although the estimation remains stable when changing directions, the AUV does not use this estimation of the currents to navigate. This results in an offset from the desired path.

With the new EKF without the modified controller there is clearly an offset from the path when travelling in the east and west directions. This corresponds to when the cross-current is higher, thus affecting the navigation more. Correspondingly, there is a smaller offset when travelling in the north and south directions. To correct for this navigational deficiency, the modified MOOS heading controller was implemented. With the simulation results in Figure 3.11 it can be seen that the combination of the new EKF and compensated MOOS heading controller improves the estimation and navigation from the previously used EKF and MOOS controller. This approach eliminates the transient when changing directions while utilizing the estimated currents to help the AUV converge to the desired path.

From these simulations it can be seen that the new EKF has comparable estimation accuracy both with and without current. This suggests that the EKF will remain stable and accurate in any encountered constant current. Although the EKF may be accurate, there is the physical limitation on the currents that the AUV can operate in. This is due to the limit on the AUV relative speed, with which a higher current would prevent the AUV from making headway. Also, as stated earlier, the MOOS adaption calculation cannot be made if the current is higher than the relative speed.

These results demonstrate that it is plausible to utilize an EKF for real-time estimation and control in the presence of currents without additional sensors. This approach shows successful estimation of the encountered currents based solely on the positional bias between the measurements and state propagation. Additionally, the use of these estimated currents to adjust the MOOS heading controller to navigate in the presence of these unknown currents is

shown to be effective. The large improvement of this method of estimating the unknown currents over the previous EKF that captured the effects as a speed and heading bias is the global reference frame that prevents divergence when the AUV changes heading.

### **3.4 Estimation and Navigation Field Testing Results**

As the objective of this research is a real-time implementation of the EKF and controller modifications on the AUVs to help make the desired scientific measurements in oceanic environments, field testing is critical. Though simulations can be useful for investigating stability and covariance interplay, field testing may expose shortcomings. Due to simplifications used in simulation as well unmodeled phenomena, simulations don't capture many important aspects of the real-time implementation.

To test the effectiveness of the new EKF and MOOS heading controller, field testing was conducted at ARD utilizing the acoustic tracking range. With the assumption that this tracking system is highly accurate, the position estimation from this system was held as true and used for comparison to establish an error metric. This was used to compare results against field tests with previous EKFs.

#### **3.4.1 Zero Current**

As stated above, the field testing was first conducted without a substantial current. This is desired as much of the preliminary testing is performed in a lake environment. For this zero current testing, the modification to the heading controller should have minimal effect as the estimated currents should be negligible except during the transient at the start of the mission.

The field testing data presented in Figure 3.12 shows typical LBL results with the new EKF combined with the modified MOOS heading controller. For these tests, the navigation utilizes ranges to four Hydroid transponders that are anchored on the day.

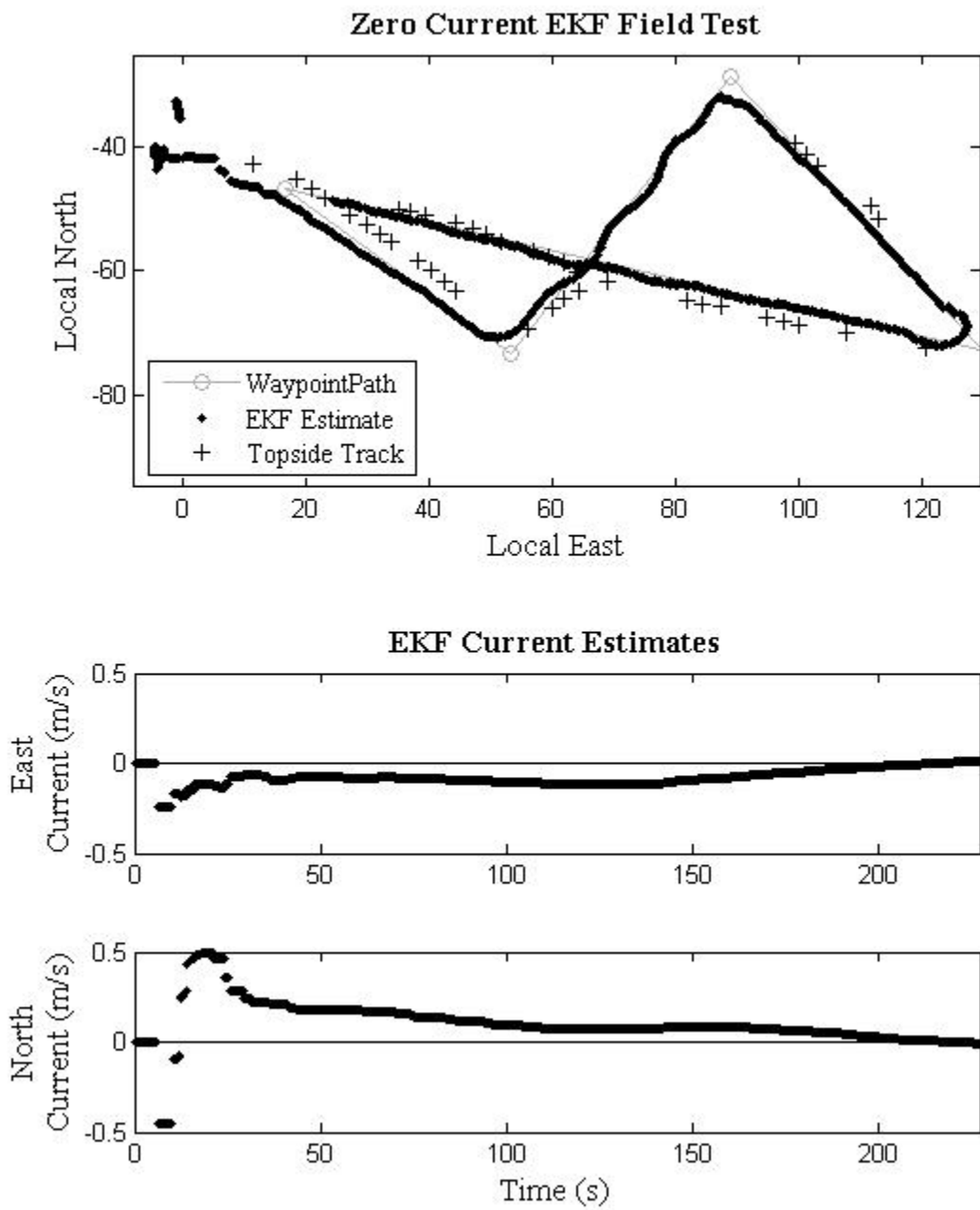


**Figure 3.12:** Field test of the new EKF in zero current.



As can be seen in Figure 3.12, there is a significant portion of the course that has no corresponding topside track. This is believed to be due to the attached preamplifier acoustically shadowing enough of the topside tracking transponders to prevent a position solution. Due to this, the presented results may be slightly biased.

From this test, it was confirmed that the speed correlation is inadequate when cornering. This is exacerbated during sharp corners such as at the far east end of the course. As the speed measurement is based solely on the RPM correlation and the RPM is constant during a mission, the EKF is fed a constant speed measurement. In actuality, the AUV slows significantly when cornering. This induces a significant bias after the sharp corner, where the EKF estimate gets ahead of the actual position. The estimation starts to reconverge, yet due to the covariance interactions, this takes a significant amount of time.

Although there is a significant error introduced by this speed correlation problem, the EKF seems to work well overall. The estimated currents are fairly stable and near zero, as expected. As no true measure of current was available, the estimated current cannot be fully validated. Table 3.3 shows the average EKF estimation and off-path errors for each leg of the course as well for the total mission. For these calculations, the position solutions before the first waypoint are not used as there is no corresponding known path.

**Table 3.3:** EKF estimation error and off-path error during zero current field test.

	<b>Estimation Error</b>	<b>Off-Path Error</b>
<b>Leg 1</b>	4.43m	2.93m
<b>Leg 2</b>	2.20m	1.17m
<b>Leg 3</b>	1.85m	1.23m
<b>Leg 4</b>	9.23m	1.70m
<b>Total</b>	6.29m	1.93m

As can be seen in Table 3.3 above, the estimation and off-path errors are not as accurate as anticipated from the simulation. An interesting observation is the trend with the accuracy of the EKF estimation. It can be seen that the EKF estimation gets sequentially better until the sharp corner at the east end of the course seen in Figure 3.12. This points to the EKF converging

to the true position, albeit slower than desired. When the AUV takes the sharp corner, there is a large divergence between the estimated and true positions. Although the estimation error is large for the last leg, this error is mostly along the path. This is corroborated by the off-path error that remains relatively small for this leg.

When compared to previous field testing results, the accuracy is significantly diminished. From [17] a previous EKF estimation had an RMS error of 1.60 m. This is significantly better than the 6.29 m seen in the field testing for the new EKF. Some of this error is likely due to sharp corner at the east end of the track, which was not part of the course used for the previously reported field testing. As can be seen from the third leg in Table 3.3, the accuracy of this new EKF is comparable to that of the previous EKF. This suggests that a longer course, without sharp corners, may significantly reduce the estimation inaccuracy.

### 3.4.2 Simulated Current

To induce a simulated current biases were incorporated into the propagation model. These biases were  $c_{ESIM} = 0.15$  m/s and  $c_{NSIM} = 0.6$  m/s. With these biases, the new EKF should estimate currents of the same magnitude. Utilizing these estimated current components, the adaption to the MOOS heading controller will attempt to compensate for a current that doesn't physically exist. Using the calculations from the compensated MOOS controller, it is possible to calculate a steady-state offset that the AUV should navigate towards. Figure 3.13 shows a field test conducted with this simulated current. Along with the programmed waypoint course, the theoretical steady-state offset from this path is included.

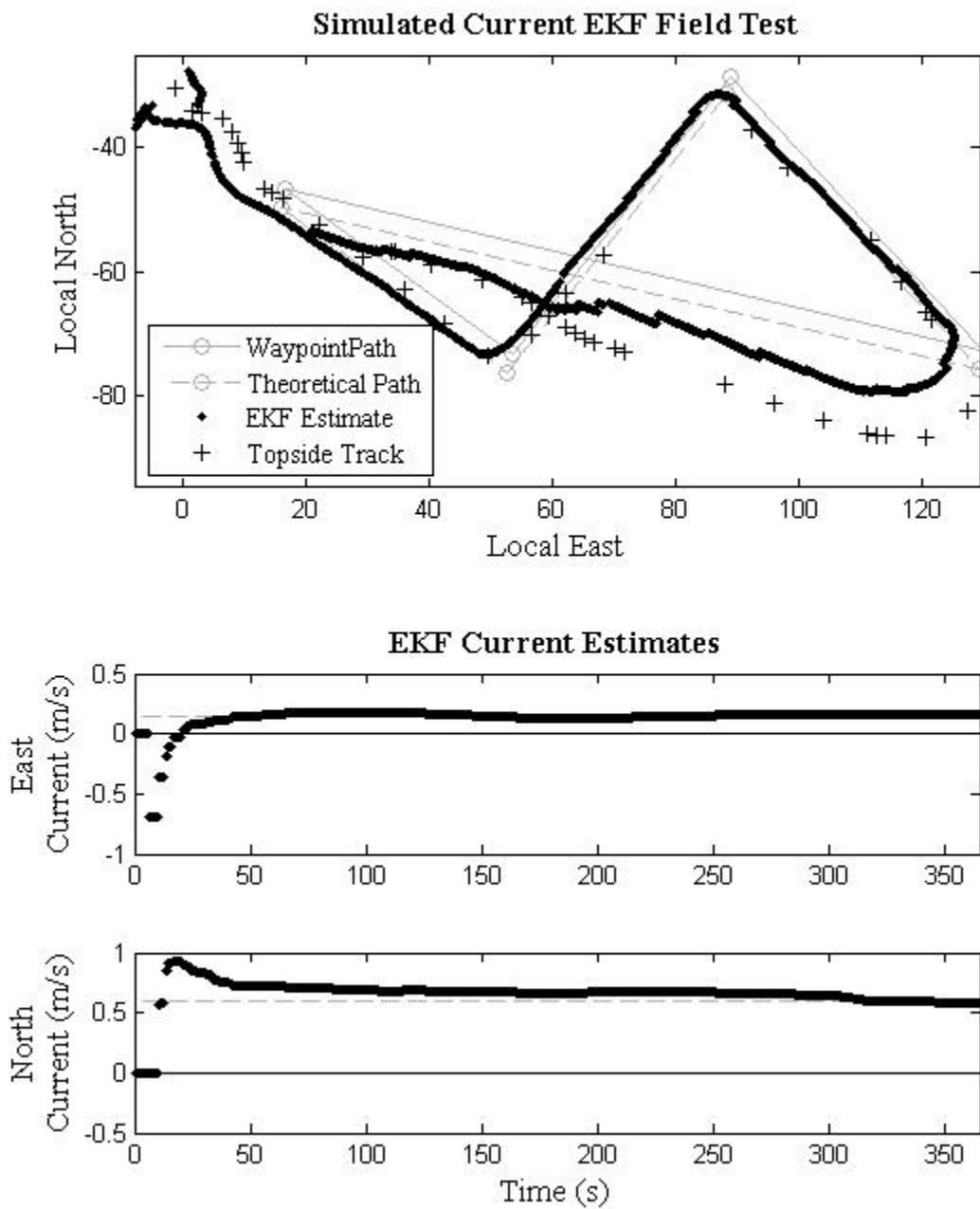


**Figure 3.13:** Field test of the new EKF with modified MOOS controller using a simulated current.

As can be seen in Figure 3.13, the AUV tends to converge to this theoretical path. Although this converges as expected, the time for this convergence to occur takes much longer than is desired. Along with this slow convergence, there is a large estimation divergence on the last corner of the mission. This is believed to be due to the modified MOOS heading controller attempting to account for the effects of an estimated current that is not physically there. It is expected that in the presence of an actual current this peculiarity will not be encountered, and behaviour will be similar to the zero current case.

Like with the zero current case, the estimation and off-path error were analyzed. As it was expected that the implemented adapted MOOS controller would drive the AUV to a steady-state offset, this theoretical path was used as the set path. Table 3.4 below shows these errors. As it is believed that the turning was affected by the simulated current implementation, the same trends are not seen in the data. Although there does seem to be a trend towards convergence during the first two legs, a large divergence in estimation error comes at the third corner. Also, the off-path error is small for all but the last leg, where the AUV turns wide and slowly reconverges towards the path.

**Table 3.4:** EKF estimation error and off-path error during simulated current field test.

	<b>Estimation Error</b>	<b>Off-Path Error</b>
<b>Leg 1</b>	4.15m	0.93m
<b>Leg 2</b>	2.32m	0.54m
<b>Leg 3</b>	7.46m	0.61m
<b>Leg 4</b>	5.49m	9.07m
<b>Total</b>	5.27m	5.35m

Though there seems to be some peculiarities with the simulated current implementation, some important aspects were demonstrated. The EKF stably estimated the correct offsets. These estimated offsets along with the adapted MOOS heading controller navigated the AUV towards the theoretical path. This gives confidence that the changes made to the MOOS heading controller are working as expected.

## Chapter 4: Conclusions

With the extension of operations of the UI AUVs to oceanic environments, new difficulties were encountered. The most significant of these was the presence of ocean currents. A common approach to oceanic operations is using a Doppler velocity log (DVL) or similar sensors to get a direct velocity over ground (VOG) measurement. As the UI AUVs are small and inexpensive, and it is desired that they remain this way, the inclusion of additional sensors to alleviate this difficulty was and remains impractical.

With the lack of additional sensors, an estimation technique was used. This technique utilized an EKF to make a real-time estimate of the AUV state including the local ocean current. As no information about the current was available to the AUV, the current is estimated based on the discrepancy between the predicted and measured positions. The estimated current is utilized to improve navigation using a modification to the MOOS heading controller that corrects for the effect of current to navigate along the predefined waypoint course.

This approach works well in simulation. The current is estimated accurately and remains stable after converging. Additionally the modified MOOS heading controller effectively navigates along the desired path. Also, this EKF shows comparable accuracy to that seen with previous EKF schemes in the zero-current case, around 0.83 m for the new EKF and 1.34 m for the previous EKF, as well as maintaining this accuracy when encountering constant currents.

With the AUV implementation, various problems were encountered. The two main issues that arose were both with how the STW is estimated. The first of these issues has to do with the dive sequence. The dive sequence that is currently used on the AUV initially reverses and pulls the AUV underwater before stopping and transitioning to forward movement. During the dive sequence the speed estimate is hard-coded to .5 m/s forward. Although this is not an accurate speed estimate for this dive sequence, the EKF is not stabilized and thus this does not seem to make a large difference. Conversely, improving this estimate would likely help the

EKF estimate to converge quicker. The larger issue encountered has to do with the RPM correlation while the AUV turns. As the RPM is constant, the EKF is given a constant speed measurement throughout a mission. When the AUV turns, the true speed through water (STW) slows significantly. This is exacerbated with larger changes in direction. This causes a significant divergence between the EKF estimate and true positions. When this happens after the EKF has stabilized, a significant amount of time is required to reconverge.

Due to these speed measurement issues, the field tests resulted in poor estimation. Where previous research has seen estimation error as low as 1.60 m, the new EKF had an average error of 6.29 m in the zero current test. As the new EKF was tested on a course that included four sharp corners, where as the previous research was conducted on a straight course, the cornering and speed measurement may be a significant contribution to this increase in estimation error. Even with the cornering, the EKF estimation error reached as low as 1.85 m for the third leg of the course. This strongly suggests that improving the speed correlation for corners could increase the EKF accuracy. Although the accuracy of the new EKF was less than desired, the concept shows plausibility. As the focus of this research is to improve the state estimation to account for unmeasurable currents, the initial results are promising. In both the simulation and field testing the EKF accurately estimated the unknown currents. With this aspect of the EKF working well, it is plausible that tuning the covariance matrices along with a better speed correlation implementation could improve the accuracy of the estimation. The work presented in this paper shows that it is plausible to use this EKF and modified MOOS heading controller to improve operations of the UI AUVs in oceanic environments. With additional research the accuracy of this EKF scheme is expected to be improved without degrading stability.

Once the EKF estimate is within the desired accuracy, the extension to use with chained missions will be trivial. The chained mission continuous EKF worked well other than the speed measurement issues in field testing. Once these issues are accounted for, it is believed that the EKF will be able to accurately estimate the AUV state throughout a set of chained missions. This can significantly improve operations in an oceanic environment.

In addition to the state estimation and navigation, the control gains were investigated for higher speed operation. Using a simulation and subsequent field testing, the depth control was improved significantly. With the new gains of  $P_z = -0.1$  and  $P_\theta = 2.0$ , the AUV oscillated at about 44% of the RMS amplitude that was seen with the previous standard gains in field testing. Although the standard heading gain was not changed from  $P_\psi = -0.3$ , the roughly  $5^\circ$  RMS amplitude of heading oscillation is sufficient for AUV operations. With these gains the AUVs are expected to be able to operate effectively at higher steady-state speeds, allowing for operations in more substantial ocean currents.

## 4.1 Future Work

### 4.1.1 CFD Model

To improve the simulation for the AUV control gains, a CFD model is being developed. Ahmad Hazem Hammad with mentorship from Dr. Xing, a graduate student and a professor in the Mechanical Engineering Department, respectively, are investigating the force and drag coefficients at various angles of attack. The current model is using a simplified geometry that only included the hull of the AUV. As research progresses, it is desired to evolve the CFD model to include the entire AUV geometry with externally mounted components.

An accurate CFD model would allow for precise analysis into the effects of the angle of attack and side slip of the AUV during various realistic scenarios. This could be utilized to create an accurate simulation to investigate the control gain effects. Ideally this simulation will be realistic enough to incorporate dynamic effects. This would significantly increase the usefulness of the simulation to investigate the effects of various control gains.

### 4.1.2 Speed Correlation

As stated previously, the speed correlation used on the AUV is insufficient during cornering. The speed correlation uses only the commanded RPM to estimate the AUV speed. When the AUV changes directions, the AUV slows significantly. This causes the estimated

speed to diverge significantly from the true AUV speed. This introduces a large error in the EKF position estimate.

To remedy this speed correlation, the CFD model detailed above might be useful to estimate the side-slip during cornering. This combined with an IMU measured turning rate may give an accurate speed during cornering. Additionally, including a deadband below a set RPM or going to a higher order correlation for a larger range of RPM values could be an improvement. With an improved speed estimate throughout the mission, the EKF estimate could be significantly improved.

Additionally, field testing could be performed to generate estimates of the AUV speed based on set rudder angle. This would require using the acoustic tracking range at ARD while operating the AUVs in circles with a set rudder angle. This would give reasonable estimates of the speed while the AUVs are turning. Although this would be much improved from the current speed correlation, it would still not account for dynamic effects. One way to alleviate this shortcoming would be to use the covariance matrices as detailed below.

#### 4.1.3 Covariance Matrices

With the field testing, the initial convergence took significantly longer than is desired. As stated earlier, this may be reduced with better speed measurement, yet this will likely not reduce the convergence time to an acceptable level. To further reduce this time, the interactions between the various covariance matrices will need to be further investigated. Although the covariance values were estimated off field test data, there is room for improvement.

The noise values associated with the propagation model were estimated based on typical error bounds associated with the various simplifications. Determining a more precise error bound associated with this specific system may improve the convergence. Likewise, a more detailed analysis of the various measurement covariances could be conducted. As the heading and speed measurements are assumed to have a constant covariance throughout the mission, the EKF trusts these measurements even during cornering. A highly detailed approach could use a



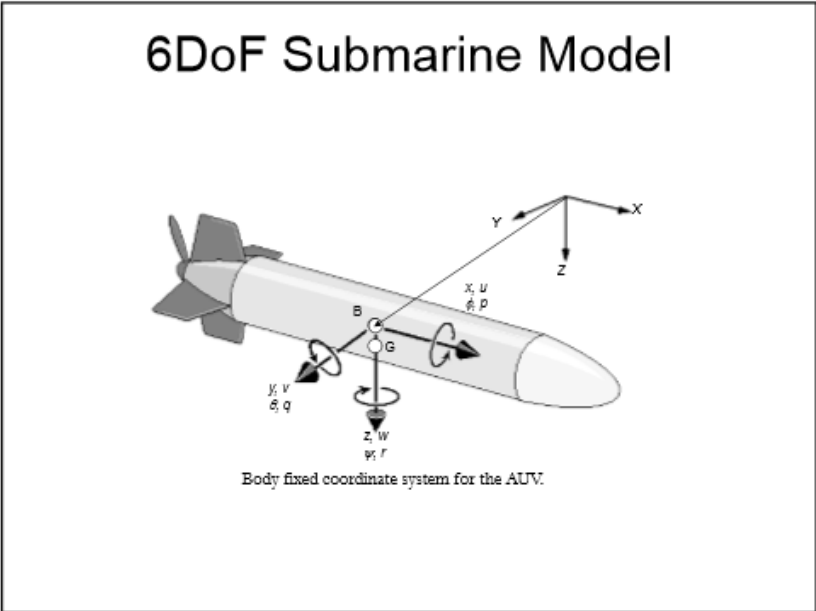
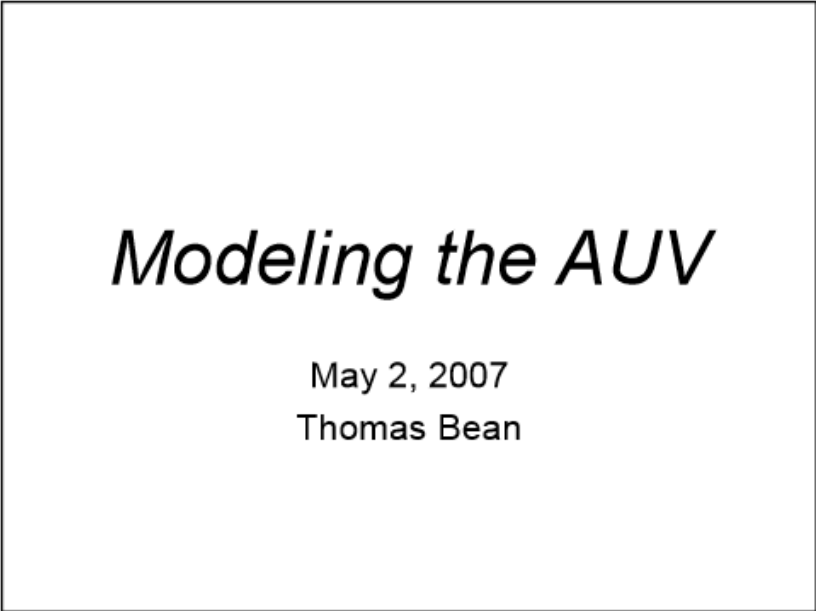
time-dependent covariance value. Utilizing the on-board IMU, the rate of turning could be used to adapt the covariance value. This approach would require significant field testing to establish a correlation between the rate of turning and the associated covariance on the measurement. Using this approach could reduce the inaccuracies induced by the poor speed measurement during cornering. Additionally, an increase in the covariance during turning could account for the difference between a steady-state turning speed and a dynamic turning speed, as mentioned above. Although this approach would likely increase the estimation accuracy, there would be a significant increase in the complexity of the EKF implementation.

## References

- [1] P. M. Newman, "MOOS - A Mission Oriented Operating Suite," Department of Ocean Engineering, Massachusetts Institute of Technology, Tech. Rep., OE2003- 07, 2003.
- [2] B. Armstrong, J. Pentzer, D. Odell, T. Bean, J. Canning, D. Pugsley, J. Frenzel, M. Anderson, and D. Edwards, "Field Measurement of Surface Ship Magnetic Signature using Multiple AUVs," in *IEEE OCEANS '09*, Biloxi, MS, USA, 2009.
- [3] B. Armstrong, E. Wolbrecht, and D.B. Edwards, "AUV Navigation in the Presence of a Magnetic Disturbance with an Extended Kalman Filter," *Proceedings of Oceans '10 IEEE Sydney*, Sydney, Australia, May 24-27, 2010.
- [4] E. Wolbrecht, M. Anderson, J. Canning, D. Edwards, J. Frenzel, D. Odell, T. Bean, J. Stringfield, J. Fuesi, B. Armstrong, A. Folk, B. Crosbie, "Field Testing of Moving Short-Baseline Navigation for Autonomous Underwater Vehicles using Synchronized Acoustic Messaging," *The Journal of Field Robotics*, Vol. 30, No. 4, pp. 519-535, 2013.
- [5] E. Wolbrecht, B. Gill, R. Borth, J. Canning, M. Anderson, D. Edwards, "Hybrid Baseline Localization for Autonomous Underwater Vehicles," *Journal of Intelligent and Robotic System (JINT)*, pp. 1-19, 2014.
- [6] D. Rudolph and T. Wilson, "Doppler Velocity Log Theory and Preliminary Considerations for Design and Construction," in *Southeastcon, 2012 Proceedings of IEEE*, pp. 1-7.
- [7] A. P. Aguiar and A. M. Pascoal, "Dynamic Positioning and Way-Point Tracking of Underactuated AUVs in the Presence of Ocean Currents," *International Journal of Control*, vol. 80, no. 7, pp. 1092-1108, Jul. 2007.
- [8] A. J. Healey, P. E. An, and D. B. Marco, "On Line Compensation of Heading Sensor Bias for Low Cost AUVs," In *Proceedings of the 1998 Workshop on Autonomous Underwater Vehicles*, pages 35-42, August 1998.
- [9] B. Garau, M. Bonet, A. Alvarez, S. Ruiz, and A. Pascual, "Path Planning for Autonomous Underwater Vehicles in Realistic Oceanic Current Fields: Application to Gliders in the Western Mediterranean Sea," *Journal of Maritime Research*, vol. 6, no. 2, pp. 5-22, 2009.
- [10] D. Rao and S. B. Williams, "Large-Scale Path Planning for Underwater Gliders in Ocean Currents," in *Australasian Conference on Robotics and Automation (ACRA)*, 2009.
- [11] K. Teo, E. An, and P. P. J. Beaujean, "A Robust Fuzzy Autonomous Underwater Vehicle (AUV) Docking Approach for Unknown Current Disturbances," *IEEE Journal of Oceanic Engineering*, vol. 37, no. 2, pp. 143-155, Apr. 2012.
- [12] J. Vaganay, P. Baccou, and B. Jouvencel, "Homing by Acoustic Ranging to a Single Beacon," in *OCEANS 2000 MTS/IEEE Conference and Exhibition*, 2000, pp. 1457-1462.

- [13] A. S. Gadre and D. J. Stilwell, "A Complete Solution to Underwater Navigation in the Presence of Unknown Currents Based on Range Measurements from a Single Location," in *Proc. of the IEEE International Conference on Intelligent Robots and Systems*, Edmonton, Alberta, Canada, 2005, pp. 1420-1425.
- [14] D. J. Stilwell, A. S. Gadre, C. A. Sylvester, and C. J. Cannell, "Design Elements of a Small Low-Cost Autonomous Underwater Vehicle for Field Experiments with Multi-Vehicle Coordination," in *Proceedings of the IEEE Workshop on Autonomous Underwater Vehicles*, Sabasco Estates, ME, 2004.
- [15] Jordan Stringfield, "Navigation and Localization of an Autonomous Underwater Vehicle Fleet for Magnetic Field Measurements," University of Idaho, Moscow, Master's Thesis 2012.
- [16] J. Canning, M. Anderson, D. Edwards, M. O'Rourke, T. Bean, and J. Pentzer, "A Low Bandwidth Acoustic Communication Strategy for Supporting Collaborative Behaviors in a Fleet of Autonomous Underwater Vehicles," *US Navy Journal of Underwater Acoustics*, vol. 59, no. 3, pp. 285-299, July 2009.
- [17] Christopher Walker, "Magnetic Signature Mapping of a Moving Ship Using a Fleet of Autonomous Underwater Vehicles", University of Idaho, Moscow, Master's Thesis 2012.
- [18] D. Schipf, J. Feusi, M. Anderson, E. Wolbrecht, J. Canning and D. Edwards, "Using AUV-Acquired Survey Data to Derive a Magnetic Model for a Surface Vessel," *2013 OCEANS - San Diego*, San Diego, CA, 2013, pp. 1-8.
- [19] R. E. Kalman, "A New Approach to Linear Filtering and Prediction Problems." *Journal of basic Engineering*, 82, no. 1 (1960): 35-45.
- [20] R. E. Kalman, "Contributions to the Theory of Optimal Control," *Boletin Sociedad Matematica Mexicana*, 5, 1960, 102-119.
- [21] D. Simon, *Optimal State Estimation: Kalman, H Infinity and Nonlinear Approaches*: Wiley-Interscience, 2006.
- [22] D. Odell, J. Pentzer, J. Canning, D. Edwards, "A Versatile Tracking System for AUV Testing", *Proceedings of IEEE Oceans 2010*, Sydney, Australia, May 2010.

These slides were created by Tom Bean to detail the force and moment equations for the AUV. The simulation used to analyze the control gains was based on these equations.




## Transformation angles

$$\begin{bmatrix} \dot{x} \\ \dot{y} \\ \dot{z} \end{bmatrix} = \begin{bmatrix} \cos \psi \cos \theta & -\sin \psi \cos \phi + \cos \psi \sin \theta \sin \phi & \sin \psi \cos \phi + \cos \psi \sin \theta \cos \phi \\ \sin \psi \cos \theta & \cos \psi \cos \phi + \sin \psi \sin \theta \sin \phi & -\cos \psi \cos \phi + \sin \psi \sin \theta \cos \phi \\ -\sin \theta & \cos \theta \sin \phi & \cos \theta \cos \phi \end{bmatrix} \begin{bmatrix} u \\ v \\ w \end{bmatrix}$$

$$\begin{bmatrix} \dot{\phi} \\ \dot{\theta} \\ \dot{\psi} \end{bmatrix} = \begin{bmatrix} 1 & \sin \phi \tan \theta & \cos \phi \tan \theta \\ 0 & \cos \phi & \sin \phi \\ 0 & \sin \phi / \cos \theta & \cos \phi / \cos \theta \end{bmatrix} \begin{bmatrix} p \\ q \\ r \end{bmatrix}$$

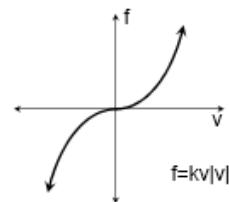
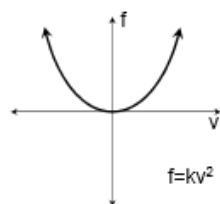
## Types of Forces

Weight =  $mg$        *Constant*

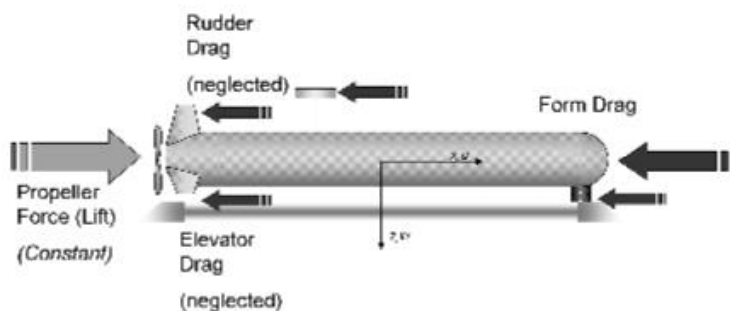
Buoyancy =  $\rho g V$        *Constant*

Drag =  $\frac{1}{2} \rho C_D A_C v^2$         $K_D v^2$  or  $K_D v|v|$

Lift =  $\frac{1}{2} \rho C_L A_S v^2$         $K_L v^2$  or  $K_L v|v|$

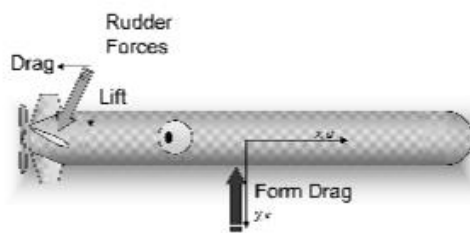


## Forces: Longitude x direction



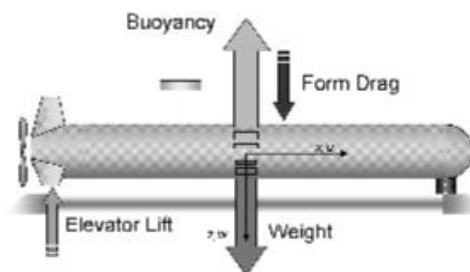
$$\Sigma F_x = -(W - B) \sin \theta - \frac{1}{2} \rho D_x A_x u |u| + F_{prop(lift)}$$

## Forces: Lateral y direction



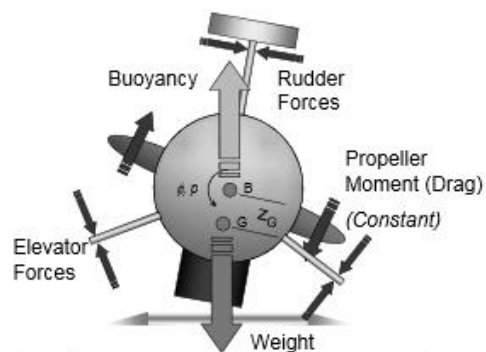
$$\Sigma F_y = (W - B) \cos \theta \sin \phi - \frac{1}{2} \rho D_y A_y v |v| + \frac{1}{2} \rho L_y A_{Rud} u |u| \delta_{Rud}$$

## Forces: vertical z direction



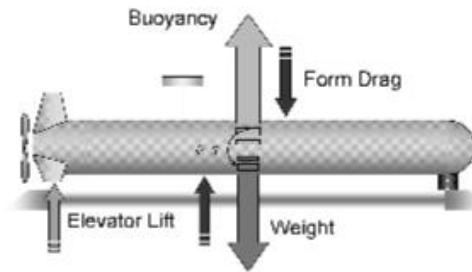
$$\Sigma F_z = (W - B) \cos \theta \cos \phi - \frac{1}{2} \rho D_z A_z w |w| + \frac{1}{2} \rho L_z A_{Elev} u |u| \delta_{Elev}$$

## Moments: Roll $\phi$



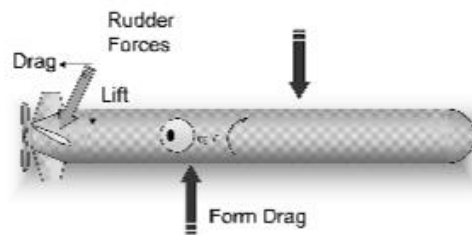
$$\Sigma M_{x,\phi} = -(W z_G) \cos \theta \sin \phi - \frac{1}{2} \rho D_\phi A_\phi p |p| + M_{prop(drag)}$$

## Moments: Pitch $\theta$



$$\Sigma M_{y,\theta} = -(W_{z_G}) \sin \theta - \frac{1}{2} \rho D_{\theta} A_{\theta} q |q| + \frac{1}{2} \rho L_z A_{Elev} u |u| \delta_{Elev} x_{Elev}$$

## Moments: Yaw $\psi$



$$\Sigma M_{z,\psi} = -\frac{1}{2} \rho D_{\psi} A_{\psi} r |r| + \frac{1}{2} \rho L_y A_{Rud} u |u| \delta_{Rud} x_{Rud}$$



## Differential Equations

Recall:

$$\mathbf{F} = m\mathbf{a} \quad \text{and} \quad \mathbf{M} = I\boldsymbol{\alpha}$$

First we will look at Forces

## Force/Moment Equations

Translation

$$\Sigma F_x = -(W - B)\sin\theta - \frac{1}{2}\rho D_x A_x u|u| + F_{prop(lift)} + \text{CROSSTERMS}$$

$$\Sigma F_y = (W - B)\cos\theta \sin\phi - \frac{1}{2}\rho D_y A_y v|v| + \frac{1}{2}\rho L_y A_{rud} u|u|\delta_{rud} + \text{CROSSTERMS}$$

$$\Sigma F_z = (W - B)\cos\theta \cos\phi - \frac{1}{2}\rho D_z A_z w|w| + \frac{1}{2}\rho L_z A_{Etv} u|u|\delta_{Etv} + \text{CROSSTERMS}$$

Rotations

$$\Sigma M_{x,\phi} = -(Wz_G)\cos\theta \sin\phi - \frac{1}{2}\rho D_\phi A_\phi p|p| + M_{prop(drag)} + \text{CROSSTERMS}$$

$$\Sigma M_{y,\theta} = -(Wz_G)\sin\theta - \frac{1}{2}\rho D_\theta A_\theta q|q| + \frac{1}{2}\rho L_z A_{Etv} u|u|\delta_{Etv} + \text{CROSSTERMS}$$

$$\Sigma M_{z,\psi} = -\frac{1}{2}\rho D_\psi A_\psi r|r| + \frac{1}{2}\rho L_y A_{rud} u|u|\delta_{rud} + \text{CROSSTERMS}$$

## Accelerations (Yikes!)

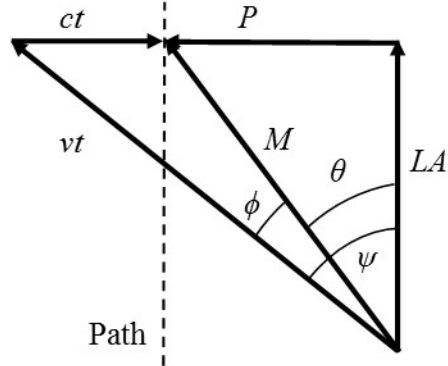
$$\begin{aligned}
 F_x &= m(\dot{u} + qw - rv - \cancel{xy}(q^2 + r^2) + \cancel{yz}(pq - \dot{r}) + z_G(pr + \dot{q})) \\
 F_y &= m(\dot{v} + ru - pw - \cancel{yz}(q^2 + r^2) + z_G(qr - \dot{p}) + \cancel{xy}(qp + \dot{r})) \\
 F_z &= m(\dot{w} + pv - qu - z_G(q^2 + r^2) + \cancel{xy}(rp - \dot{q}) + \cancel{yz}(rq + \dot{p})) \\
 M_x &= I_{xx}\dot{p} + (I_{zz} - I_{yy})qr - \cancel{yz}(qp + \dot{r}) + \cancel{xy}(rp - \dot{q}) + \dots \\
 &\quad \dots + \cancel{yz}(r^2 - q^2) + m[\cancel{xy}(\dot{w} + pv - qu) - z_G(\dot{v} + ru - pw)] \\
 M_y &= I_{yy}\dot{q} + (I_{xx} - I_{zz})rp - \cancel{xy}(rq + \dot{p}) + \cancel{yz}(pq - \dot{r}) + \dots \\
 &\quad \dots + \cancel{xy}(p^2 - r^2) + m[z_G(\dot{u} + qw - rv) - \cancel{yz}(\dot{w} + pv - qu)] \\
 M_z &= I_{zz}\dot{r} + (I_{yy} - I_{xx})pq - \cancel{xy}(pr + \dot{q}) + \cancel{yz}(qr - \dot{p}) + \dots \\
 &\quad \dots + \cancel{xy}(q^2 - p^2) + m[\cancel{yz}(\dot{v} + ru - pw) - \cancel{xy}(\dot{u} + qw - rv)]
 \end{aligned}$$

## Accelerations (Better!)

$$\begin{aligned}
 F_x &= m(\dot{u} + qw - rv + z_G(pr + \dot{q})) \\
 F_y &= m(\dot{v} + ru - pw + z_G(qr - \dot{p})) \\
 F_z &= m(\dot{w} + pv - qu - z_G(q^2 + r^2)) \\
 M_x &= I_{xx}\dot{p} + (I_{zz} - I_{yy})qr + m[-z_G(\dot{v} + ru - pw)] \\
 M_y &= I_{yy}\dot{q} + (I_{xx} - I_{zz})rp + m[z_G(\dot{u} + qw - rv)] \\
 M_z &= I_{zz}\dot{r} + (I_{yy} - I_{xx})pq
 \end{aligned}$$

## Appendix B: Modified MOOS Heading Controller Calculation

Shown here is the derivation of the modified MOOS heading controller. For implementation, only Equations (11) to (13) are needed.



### Variables:

- $M$  = original MOOS heading vector
- $LA$  = look-ahead vector
- $P$  = off-path vector
- $t$  = unknown effective time
- $vt$  = estimated AUV velocity times  $t$
- $ct$  = estimated cross current velocity time  $t$
- $\theta$  = original MOOS heading
- $\phi$  = unknown compensation heading
- $\psi$  = new MOOS heading

### Derivation:

Form the law of cosines,

$$|ct|^2 = |vt|^2 + |M|^2 - 2|vt||M| \cos \phi. \quad (1)$$

By the definition of the dot product,

$$vt \cdot M = |vt||M| \cos \phi. \quad (2)$$

Substituting Eq. (2) into Eq. (1) gives

$$|ct|^2 = |vt|^2 + |M|^2 - 2(vt \cdot M). \quad (3)$$

From vector addition we can say that

$$vt = LA + P - ct, \quad (4)$$

and

$$M = LA + P. \quad (5)$$

Then,

$$v_t \cdot M = (LA + P - ct) \cdot (LA + P) = |LA|^2 + |P|^2 - |ct||P|. \quad (6)$$

Using the Pythagorean theorem,

$$|M|^2 = |LA|^2 + |P|^2. \quad (7)$$

Substituting Eq. (7) into Eq. (6) gives

$$vt \cdot M = |M|^2 - |ct||P|. \quad (8)$$

Substituting Eq. (8) into Eq. (3) gives

$$|ct|^2 = |vt|^2 + |M|^2 - 2|M|^2 + 2|ct||P|. \quad (9)$$

As  $t$  is a constant, we can pull it out. Then setting equal to 0, we get

$$0 = (|v|^2 - |c|^2)t^2 + 2|c||P|t - |M|^2. \quad (10)$$

Using the quadratic formula to solve for  $t$ , keeping only the positive solution, gives

$$t = \frac{-2|c||P| + \sqrt{(2|c||P|)^2 + 4(|v|^2 - |c|^2)|M|^2}}{2(|v|^2 - |c|^2)}. \quad (11)$$

With this solution of  $t$ , we can get

$$vt = M - ct. \quad (12)$$

The angle of this vector,  $vt$  is the new target heading;

$$\angle vt = \theta + \phi = \psi. \quad (13)$$